JNeurosci Accepted Manuscript

JNeurosci
THE JOURNAL OF NEUROSCIENCE

Research Articles: Neurobiology of Disease

Risperidone ameliorates prefrontal cortex neural atrophy and oxidative/nitrosative stress in brain and peripheral blood of rats with neonatal ventral hippocampus lesion

https://doi.org/10.1523/JNEUROSCI.1249-19.2019

Cite as: J. Neurosci 2019; 10.1523/JNEUROSCI.1249-19.2019

Received: 29 May 2019
Revised: 7 August 2019
Accepted: 31 August 2019

This Early Release article has been peer-reviewed and accepted, but has not been through the composition and copyediting processes. The final version may differ slightly in style or formatting and will contain links to any extended data.

Alerts: Sign up at www.jneurosci.org/alerts to receive customized email alerts when the fully formatted version of this article is published.

Copyright © 2019 the authors

JNeurosci Accepted Manuscript

Submitted to Journal of Neuroscience

Risperidone ameliorates prefrontal cortex neural atrophy and oxidative/nitrosative stress in brain and peripheral blood of rats with neonatal ventral hippocampus lesion.

Hiram Tendilla-Beltrán[1,2,3,4], Silvia Meneses-Prado[1], Rubén Antonio Vázquez-Roque[1], Miguel Tapia-Rodríguez[5], Andrea Judith Vázquez-Hernández[1], Heriberto Coatl-Cuaya[1,2], David Martín-Hernández[3,4,6,7], Karina S. MacDowell[3,4,6,7], Linda Garcés-Ramírez[2], Juan C. Leza[3,4,6,7,*], Gonzalo Flores[1,**]

[1]Instituto de Fisiología, Benemérita Universidad Autónoma de Puebla (BUAP), Puebla, 72570, Mexico

[2]Departamento de Fisiología, Escuela Nacional de Ciencias Biológicas, Instituto Politécnico Nacional (IPN), CDMX, 11340, Mexico.

[3]Departamento de Farmacología y Toxicología, Facultad de Medicina, Universidad Complutense de Madrid (UCM), Madrid, 28040, Spain.

[4]Instituto Universitario de Investigación en Neuroquímica, Universidad Complutense de Madrid (IUIN-UCM), Madrid, 28040, Spain.

[5]Instituto de Investigaciones Biomédicas, Universidad Nacional Autónoma de México (UNAM), CDMX, 04510, Mexico.

[6]Centro de Investigación Biomédica en Red de Salud Mental (CIBERSAM), Madrid, 28029, Spain.

[7]Instituto de Investigación Sanitaria Hospital 12 de Octubre (I+12), Madrid, 28041, Spain.

* Correspondence to: Juan Carlos Leza, Departamento de Farmacología y Toxicología, Facultad de Medicina, Universidad Complutense de Madrid, Avenida Complutense s/n, 28040, Madrid, España. E-mail: jcleza@med.ucm.es

**Correspondence to: Gonzalo Flores, Instituto de Fisiología, Benemérita Universidad Autónoma de Puebla, 14 Sur 6301, Puebla, México, CP 72570. E-mail: gonzaloflores56@gmail.com

Manuscritp: 38 pages, 11 figures, 1 table, abstract 145 words, significance statement 115 words, introduction 646 words, discussion 1449 words.

Conflict of interest: The authors declare no competing financial interests.

JNeurosci Accepted Manuscript

Aknowledgements: The authors want to thank Francisco Ramos Collazo for his help with the animal care and Sandra Rodríguez-Maus for her help with the biochemical experiments. HTB and HCC acknowledge to CONACYT for scholarship. RAVR, MTR, LG and GF acknowledge the “Sistema Nacional de Investigadores” of Mexico for memberships. Thanks to Professor Robert Simpson for editing the English language text. The funding of this study was provided by Spanish Ministry of Economy, Industry and Competitiveness (MINECO-EU-FEDER) SAF2016-75500-R to JCL and PRODEP (CA-BUAP-120) and the CONACYT grant (No. 252808) to GF. None of the funding institutions had any further role in the study design, the collection of data, analyses, and interpretation of data, writing of the report or in the decision to submit the paper for publication and interpretation of data, writing of the report or the decision to submit the paper for publication.

Running title: Risperidone and animal model of schizophrenia

JNeurosci Accepted Manuscript

Abstract

Reduction of the dendritic arbor length and the lack of dendritic spines in the pyramidal cells of the prefrontal cortex (PFC) are prevalent pathological features in schizophrenia (SZ). Neonatal ventral hippocampus lesion (NVHL) in male rats reproduces these neuronal characteristics and here we describe how this is a consequence of BDNF/TrkB pathway disruption. Moreover, COX-2 pro-inflammatory state, as well as Nrf-2 antioxidant impairment, triggers oxidative/nitrosative stress, which also contributes to dendritic spine impairments in the PFC. Interestingly, oxidative/nitrosative stress was also detected in the periphery of NVHL animals. Furthermore, risperidone treatment had a neurotrophic effect on the PFC and antioxidant effects on the brain and periphery of NVHL animals; these cellular effects were related to behavioral improvement. Our data highlight the link between brain development and immune response, as well as several other factors in order to understand mechanisms related to the pathophysiology of SZ.

JNeurosci Accepted Manuscript

Significance

Prefrontal cortex dysfunction in schizophrenia can be a consequence of morphological abnormalities and oxidative/nitrosative stress, among others. Here, we detailed how impaired plasticity-related pathways and oxidative/nitrosative stress are part of the dendritic spine pathology and their modulation by atypical antipsychotic risperidone treatment in rats with neonatal ventral hippocampus lesion. Moreover, we found that animals with neonatal ventral hippocampus lesion had oxidative/nitrosative stress in the brain as well as in the peripheral blood, an important issue for the translational approaches of this model. Then, risperidone restored plasticity and reduced oxidative/nitrosative stress of PFC pyramidal cells, and ultimately improved the behavior of lesioned animals. Moreover, risperidone had differential effects than the brain on peripheral blood oxidative/nitrosative stress.

JNeurosci Accepted Manuscript

Introduction

In 1972 Frederick Plum referred to schizophrenia (SZ) as “the graveyard of the neuropathologists”, because of the lack of determinant pathophysiological data (Plum, 1972). More than four decades later, the etiology and mechanisms of the disease are still unclear, in spite of the many approaches that have been made in order to clarify it. Interestingly, the reduction of the dendritic arbor length and the lack of dendritic spines in the pyramidal cells of the prefrontal cortex (PFC) are prevalent pathological features (Garey et al., 1998; Glantz and Lewis, 2000; Konopaske et al., 2018). Many studies in SZ focus on the PFC because of its relation to cognitive functions that allow the individuals an adequate perception of the reality and a proper behavioral response. Since dendrites and dendritic spines are the main sites for excitatory synapses in the central nervous system (CNS) (Harris and Kater, 1994), their reduction alters PFC function in SZ, triggering various characteristic symptoms: psychosis, hallucinations, and anhedonia (Glausier and Lewis, 2013). It has been proposed that excessive synaptic pruning is the cause of the dendrites and spines lost in SZ and recent studies show that this could be a microglia-mediated phenomenon, due to complement activity or phagocytosis (Sekar et al., 2016; Sellgren et al., 2019). The aforementioned highlights the immune system as a potential link between early life insults in brain development and their late consequences, which finally onsets the disease (neurodevelopmental hypothesis of SZ) (Weinberger, 1987; Potkin et al., 2009).

High levels of pro-inflammatory cytokines and immune markers, as well as an unbalanced inflammatory response in the peripheral blood of patients, have been detected (Garcia-Bueno et al., 2014b; Garcia-Bueno et al., 2014a; Leza et al., 2015; Dickerson et al., 2016). Also, post-mortem studies have shown oxidative/nitrosative stress in the PFC (Andreazza et al., 2010; Andreazza et al.,

JNeurosci Accepted Manuscript

2013; Garcia-Bueno et al., 2016). Thus inflammation and oxidative/nitrosative stress also are implicated in the pathophysiology of SZ.

The neonatal ventral hippocampus lesion (NVHL) in the rat is an useful animal model to study some mechanisms involved in the pathophysiology of SZ. Adult NVHL animals have dendritic arbor and spine pathology (Flores et al., 2005; Ryan et al., 2013; Tendilla-Beltran et al., 2019), as well as oxidative/nitrosative stress in the PFC (Cabungcal et al., 2014). These cellular impairments result in various behavioral SZ-related abnormalities such as hyperlocomotion after exposure to dopaminergic agonists or a novel environment (Lipska et al., 1993; Flores et al., 1996; Alquicer et al., 2004), altered sensory gating (Le Pen et al., 2003; McDannald et al., 2011; Vazquez-Roque et al., 2012), and social isolation (Le Pen et al., 2000; Alquicer et al., 2008; Vazquez-Roque et al., 2012). Additionally, some of these brain and behavioral alterations can be reversed by antipsychotics (Sams-Dodd et al., 1997; Rueter et al., 2004; Bringas et al., 2012; Castellano et al., 2013).

Risperidone (RISP) is an atypical antipsychotic widely used in SZ therapy. In addition to its canonical antipsychotic pharmacological mechanism (dopamine D2 and serotonin 5-HT2A receptor antagonism) (Kuroki et al., 2008), there is evidence that RISP modulates the inflammatory response. *In vitro* protocols have demonstrated that RISP treatment increases the levels of anti-inflammatory cytokines and reduces pro-inflammatory cytokines (Al-Amin et al., 2013; Brinholi et al., 2016). This effect has also been reported in patients, and also this substance decreases oxidative/nitrosative stress (Noto et al., 2014; Juncal-Ruiz et al., 2018). Even in an animal model of neuroinflammation, RISP was capable of reducing both inflammatory mediators and oxidative/nitrosative stress in the PFC (MacDowell et al., 2013).

In this study, we aim to determine the effects of RISP treatment on rats subjected to the SZ-like experimental model: the NVHL. For this purpose, we evaluated neuronal morphology and dendritic spine dynamics in the PFC. Furthermore, we

JNeurosci Accepted Manuscript

studied inflammatory parameters and oxidative/nitrosative stress in the brain and peripheral blood. Finally, we also explored possible behavioral effects of RISP in rats with NVHL.

MATERIALS AND METHODS

Animals

Pregnant Sprague-Dawley dams (n = 10) with 14-16 gestational days were obtained from our facilities (Autonomous University of Puebla and Harlan Ibérica, Spain). Animals were individually housed in a temperature/humidity controlled environment in a 12:12 h light:dark cycle with free access to food and water. After birth, considered postnatal day (PD) 0, at PD7 only male pups (n = 68) were randomly assigned for either sham (n = 34) or NVHL surgery (n = 34). On PD21, animals were weaned and a similar number of sham and lesioned rats were placed in each cage (four animals per cage). At PD89, the locomotor behavior of a group of animals (n = n = 24 sham and 24 NVHL) was evaluated. After this, all animals were administered with vehicle or RISP for 21 consecutive days. After treatment, the animals that were previously behaviorally tested were evaluated again for motor activity and social behavior. The morphological assessments were explored in these animals. Another group of animals (sham n = 10, NVHL n = 10) was sacrificed immediately after treatment for the biochemical experiments (**Fig. 1A**). All procedures described in the present study were performed in accordance with the BUAP Animal Care Committee (FLAG- UALVIEP-17-1) and the “Guide for Care and Use of Laboratory Animals” of the Mexican Council for Animal Care (Norma Oficial Mexicana NOM-062-ZOO-1999), as well as the Animal Welfare Committee of Universidad Complutense in accordance with European legislation (2010/63/EU). All efforts were made to reduce the number of animals used and minimize animal suffering in the experiments.

Surgical Procedures

JNeurosci Accepted Manuscript

Neonatal ventral hippocampus lesion protocol has been precisely described before (Lipska et al., 1993; Flores et al., 1996). On PD7, male pups (weighing 15-18 g) were anesthetized using hypothermia. Then pups were positioned on a modified platform (Sierra et al., 2009) fixed to a stereotaxic Kopf instrument, and subsequently 0.3 µl of ibotenic acid (10 µg/µl; Sigma, St. Louis, MO) or an equal volume of vehicle (0.1 M phosphate-buffered saline [PBS], pH 7.4) was bilaterally injected into the ventral hippocampus over a 2 min period through a 30-G stainless-steel cannula connected to an infusion pump through a Hamilton syringe positioned at the following coordinates: AP -3.0 mm, ML ±3.5 mm to bregma, and DV -5.0 mm from dura, according to the Paxinos and Watson rat brain atlas (Paxinos and Watson, 1986). After the procedure, pups were placed on a heating pad for recovery and returned to their dams.

Risperidone Administration

At PD90, sham and NVHL rats were administered (ip) either 0.25 mg/kg of RISP (Janssen Pharmaceutica) dissolved in 0.25% glacial acetic acid and 0.1 M PBS or vehicle for 21 consecutive days. Four groups of animals were formed (n = 17/group): 1) sham-vehicle, 2) NVHL-vehicle, 3) sham-RISP, and 4) NVHL-RISP.

Behavioral tests

Behavioral observations were carried out between 8:00-12:00 h in a noise-free, odorless room in which animals were acclimatized 24 h before tests.

Locomotor Activity. The test was performed twice: before treatment (PD89, n = 24 sham and 24 NVHL) and after RISP or vehicle administration (PD111, n = 12/group). Locomotor activity was monitored for 120 min in 16 individual cages (20 x 40 x 30 cm), each of which was equipped with eight photobeam detectors connected to a computer counter (Tecnología Digital, México). Each photobeam

JNeurosci Accepted Manuscript

interruption by the rat was counted as locomotor activity. (Morales-Medina et al., 2008).

Social interaction. One day after the post-treatment locomotor activity test, the social behavior of the animals was evaluated. The protocol was modified from the original method (File, 1980) and from a previous report from our group (Vazquez-Roque et al., 2012). Six pairs of rats from the same group (Sham-vehicle/Sham-vehicle, NVHL-vehicle/NVHL-vehicle, Sham-RISP/Sham-RISP, NVHL-RISP/NVHL-RISP) and that had no previous contact before were randomly organized and placed into an open field arena (60 x 60 x 60 cm) with dark walls. Their activity was recorded for 10 min, and videos were analyzed by a trained observer who was blind to the experiment obtaining the total number of interactions and the time spent during the active social behaviors. Only sniffing, following, grooming, mounting, wrestling, and jumping on or crawling under or over the partner behaviors were considered social behaviors.

Tissue samples

After the behavioral tests, the animals were deeply anesthetized (sodium pentobarbital 75 mg/kg, ip) and sacrificed according to the needs of the respective protocols. One group of rats were used for the Golgi-Cox method (n = 8/group), these animals were perfused intracardially with physiological saline solution and their brains were extracted and preserved in Golgi-Cox solution. Another group of rats was subjected to the stereology protocol (n = 4/group), these animals were perfused intracardially with physiological saline solution followed by 4% paraformaldehyde in 0.1 M PBS and brains were extracted and preserved in 4% paraformaldehyde. Another group of animals (n = 5/group) was used for biochemical assays. After anesthesia, intracardial blood samples were obtained and located in EDTA, then the brain was removed from the skull and the PFC was excised and frozen at -80°C until assayed.

JNeurosci Accepted Manuscript

Neuronal Morphology

Golgi-Cox stain method

To evaluate the effects of RISP on neural morphology in the PFC neurons of NVHL rats, a modified Golgi-Cox stain method was used (Gibb and Kolb, 1998). Coronal brain sections of 200 µm thickness at the level of PFC were obtained using a vibratome (Campden Instruments, MA752, Leicester, UK) and placed on clean gelatin-coated microscope slides for the revealing process: slides were treated with ammonium hydroxide (30 min in dark), then with Kodak Film Fixer (30 min in dark) and afterwards washed with distilled water, dehydrated and whitened in successive baths of 50% (1 min), 75% (1 min), 90% (1 min) and 100% (2 x 5 min) ethanol, followed by 15 min in xylene. Finally, slides were mounted with a synthetic resin medium.

Microscopic observation, Sholl analysis, dendritic spine density and classification

Bi-dimensional reconstruction of the entire basilar dendritic arbor of pyramidal PFC neurons located in layers 3 and 5 (area Cg1; plate 7-9) according to the Paxinos and Watson rat brain atlas (Paxinos and Watson, 1986), was reproduced for each neuron. For each animal, five neurons from each hemisphere were drawn using a camera lucida at 400X magnification (DMLS 2000 Leica Microscope). Dendritic tracings were quantified using Sholl analysis placing a transparent grid with equidistant (10 µm) concentric rings centered over the tracings, and the number or ring-dendrite intersections was used to estimate the total dendritic length and length per dendritic order (Sholl and Uttley, 1953). To calculate the spine density, a 30 µm approximated segment of distal dendrite was traced (at 1000X) and the number of spines was counted (to yield spines/10 µm). For dendritic spine dynamics, a hundred distal dendritic spines were manually classified (at 2000X) according to shape in six different categories: thin (elongated with similar head/neck diameter), mushroom (prominent head with defined neck), stubby

JNeurosci Accepted Manuscript

(unrecognizable neck), bifurcated (with two heads), multi-headed (more than two heads) and unclassified (without complying with any the previous criteria) (Brusco et al., 2010; Bello-Medina et al., 2016; Tendilla-Beltran et al., 2019).

Neuronal density

Stereological analysis

Before sectioning, brains were placed in a sucrose gradient and then 50 µm-thick coronal sections from PFC were obtained using a cryostat (Leica CM1510-1) and mounted on gelatin-coated microscope slides. For stereological analysis, brain-slices were stained with cresyl violet and systematically random sampled with an optical fractionator probe (Vazquez-Roque et al., 2012; Romero-Pimentel et al., 2014; Vazquez-Roque et al., 2014). Neurons were identified by their size and shape (Chareyron et al., 2012), using a MBF CX9000 color CCD camera (MicroBrightField Inc., Colchester, VT, USA) coupled to an Olympus BX51WI microscope (Olympus Corporation, Tokyo, Japan) and sampled at 60X (UPlanSAPO 60x N.A. 1.20 water immersion objective, Olympus) with the aid of StereoInvestigator v9.14.5 (MicroBrightField Inc.). Sampling parameters used for cell counting are shown in **Table 1**.

Biochemical assays

Plasma, Peripheral Blood Mononuclear Cells and PFC sample collection

Immediately after obtained, blood samples were centrifuged at 1800 rpm for 10 min at 4ºC and plasma was collected and frozen at -80ºC. The residual sample was diluted (1:1) with RPMI media and loaded into Ficoll solution (0.65 mL of Ficoll by 1 mL of sample) and centrifuged at 2000 rpm for 40 min at room temperature. Then, the mononuclear cell phase was obtained and diluted again in 15 mL of RPMI and centrifuged at 3000 rpm for 15 min at room temperature. The supernatant was

JNeurosci Accepted Manuscript

decanted and the obtained pellet was resuspended in 1 mL of RPMI and centrifuged at 3000 rpm for 10 min at room temperature. The supernatant was eliminated and the pellets, which represented the peripheral blood mononuclear cells (PBMC), were frozen at -80ºC until assayed.

Cytosolic and nuclear extraction

To obtain cytosolic fraction and nuclear extracts, a previously reported procedure was used (Martin-Hernandez et al., 2019). Shortly, PFC and PBMC samples were homogenized in 300 µl buffer [10 mmol/l N-2-hydroxyethylpiperazineN-2-ethanesulfonic acid (pH 7.9), 1 mmol/l EDTA, 1 mmol/l EGTA, 10 mmol/l KCl, 1 mmol/l dithiothreitol, 0.5 mmol/l phenylmethylsulfonyl fluoride, 0.1 mg/ml aprotinin, 1 mg/ml leupeptin, 1 mg/ml Na-p-tosyll-lysine-chloromethyl ketone, 5 mmol/l NaF, 1 mmol/l $NaVO_4$, 0.5 mol/l sucrose and 10 mmol/l Na_2MoO_4]. After 15 min, Nonidet P-40 (Roche, Germany) was added to reach a 0.5% concentration. The tubes were gently vortexed for 15 s and nuclei were collected by centrifugation at 8 000 g for 5 min. Supernatants were considered the cytosolic fraction. The pellets were resuspended in 100 µl buffer supplemented with 20% glycerol and 0.4 mol/l KCl and gently shaken for 30 min at 4 °C. Nuclear protein extracts were obtained by centrifugation at 13 000 g for 5 min and aliquots of the supernatant were stored at -80 °C.

Western blot protocol

Briefly, after quantifying and adjusting protein levels, the PFC and PBMC homogenates were mixed with Laemmli buffer (Bio-Rad, USA) and 20 µl (1 µg/µL) was loaded in acrylamide electrophoresis gel. Once the proteins were separated due their molecular weight, they were transferred to a nitrocellulose membrane (Transfer-Blot Turbo Transfer Pack, Bio-Rad) with a semi-dry transfer system (Bio-Rad). Then membranes were incubated with specifically diluted antibodies in TBS-Tween, sometimes added with bovine serum albumin (BSA): rabbit monoclonal

JNeurosci Accepted Manuscript

anti-BDNF (1:1000, Abcam, ab108319, RRID: AB_10862052), rabbit polyclonal anti-TrkB (1:1000 1% BSA, Santa Cruz Biotechnology, sc8316, RRID: AB_2155274), rabbit polyclonal anti-PI3K (1:750 1% BSA, Santa Cruz Biotechnology, sc7189, RRID: AB_2165408), rabbit polyclonal anti-Ser437phospho-Akt (1:1000, Cell Signaling, #4060, RRID: AB_2315049), rabbit polyclonal anti-Akt (1:1000, Cell Signaling, #4691, RRID: AB_915783), rabbit polyclonal anti-Thr202/Tyr204phospho-ERK (1:1000, Cell Signaling, #8544, RRID: AB_11127856), rabbit polyclonal anti-ERK (1:1000, Cell Signaling, #4695, RRID: AB_390779), rabbit polyclonal anti-IκBα (1:1000, Santa Cruz Biotechnology, sc371, RRID: AB_2235952); rabbit polyclonal anti-NF-κB p65 (1:1000, Santa Cruz Biotechnology, sc372, RRID: AB_632037), goat polyclonal anti-COX-2 (1:750 2.5% BSA, Santa Cruz Biotechnology, sc1747, RRID: AB_2084976), rabbit polyclonal anti-PPAR-γ (1:1000, Santa Cruz Biotechnology, sc7196, RRID: AB_654710), rabbit polyclonal anti-iNOS (1:750 1%BSA, Santa Cruz Biotechnology, sc650, RRID: AB_2298577), mouse monoclonal anti-4-hydroxynonenal (1:500 3% BSA, R&D Systems, MAB3249, RRID: AB_664165), goat polyclonal anti-Ser9phospho-GSK-3β (1:750 1% BSA, Santa Cruz Biotechnology, sc11757, RRID: AB_2279471); rabbit polyclonal anti-GSK-3β (1:1000, Santa Cruz Biotechnology, sc9166, RRID: AB_647604), mouse monoclonal anti-Keap1 (1:1000, R&D Systems, MAB3024, RRID: AB_2132620); rabbit polyclonal anti-Nrf2 (1:1000, Santa Cruz Biotechnology, sc722, RRID: AB_2108502). After washing with TBS-Tween solution, proteins were identified by incubating membranes with the respective horseradish peroxidase-conjugated secondary antibody (1:2000) for 90 min at room temperature and revealed by ECLTM-kit following the manufacturer's instructions (Amersham Ibérica, Spain).

Transfer blots were imaged using the Odyssey® Fc System (Li-COR Biosciences) and densitometrically quantified (NIH ImageJ® software). All densitometries are expressed in arbitrary units of optical density (O.D.). Housekeeping proteins were β-actin (1:15000, Sigma A5441, RRID: AB_476744) for cytosolic extracts and GAPDH (1:5000, Sigma G8795, RRID: AB_1078991) for nuclear ones.

JNeurosci Accepted Manuscript

Nitrites

PFC tissue were sonicated in 600 µl phosphate buffer (50 mmol/l). Nitrites (NO_2^-) were quantified in PFC homogenates and plasma using the Griess method (Green et al., 1982). In an acidic solution with 1% sulfanilamide and 0.1% N-(1-naftil) etilendiamide (NEDA), NO_2^- turned into a pink compound photometrically measured in a microplate reader at 540 nm (Synergy 2, BioTek, Germany). NO_2^- concentration in samples was calculated using a $NaNO_2$ standard curve (1-25 µM).

Lipid Peroxidation

The thiobarbituric acid method was used for lipid peroxidation determination (Das and Ratty, 1987). PFC and plasma samples were deproteinized with 40% trichloroacetic acid and HCl (5 mol/L), following the addition of 2% thiobarbituric acid (w/v) in NaOH (0.5 mol/L). The reaction was incubated in water bath at 90 ºC for 15 minutes and centrifuged at 12000 rpm for 10 min. Pink chromogen was measured in a microplate reader at 532 nm (Synergy 2, BioTek, Germany). Malondialdehyde (MDA) concentration in samples was calculated using a MDA standard curve (0-100 nM).

Protein assay

Protein levels were measured using the Bradford method based on the protein-dye binding principle (Bradford, 1976).

Statistical analyses

The mean values of each animal were treated as a single measurement for data analysis. All data are presented as the mean ± standard error of the mean (SEM). Only data on the locomotor activity before treatment were analyzed using a Mann-

JNeurosci Accepted Manuscript

Whitney *U* test. The rest of the data were analyzed using two-way ANOVA followed by the Newman-Keuls test for *post hoc* comparisons; for locomotor activity after treatment, social interaction, dendritic length, dendritic spine density, dendritic spine classification, neuronal density, and biochemical assays lesion and RISP treatment were considered as independent factors; and for length per dendritic order the independent factors were lesion and branch order. In all cases, $p < 0.05$ was considered the threshold for statistical significance. Also, p values were rounded off to 3 decimal places and when $p > 0.1$ it was just stated $p > 0.05$. Data were analyzed in Graph-Pad Prism 6.0.

RESULTS

Verification of the lesion

Coronal sections at the level of the ventral hippocampus were obtained and stained with cresyl violet (n = 68). Then, sections were analyzed and loss of hippocampal integrity was observed in rats with NVHL; only rats with hippocampal damage were used for the present study (n = 34). Sham animals (n = 34) did not show any visible damage (**Fig. 1B**).

Behavioral results

Effects of RISP on the behavioral alterations of rats with NVHL.

Locomotor activity was evaluated before and after pharmacological treatment. Before treatment, NVHL rats showed hyperactivity ($U = 144$, $p = 0.002$; **Fig. 1C**). After treatment, hyperactivity persisted in NVHL animals ($F_{(1, 44)} = 13.51$, $p < 0.001$). Also, the interaction between the lesion and RISP was significant ($F_{(1, 44)} = 4.989$, $p = 0.03$), and RISP reduced the number of movements of the NVHL animals (*post hoc*: $p < 0.05$). RISP treatment did not affect the locomotor behavior of sham animals ($F_{(1, 44)} = 2.127$, $p > 0.05$; **Fig. 1D**).

JNeurosci Accepted Manuscript

In the social test, NVHL animals spent less time in social interaction, without a RISP effect (lesion: $F_{(1, 20)}$ = 14.71, p = 0.001; RISP: $F_{(1, 20)}$ = 0.203, p > 0.05; **Fig. 1E**). There was an interaction between the lesion and RISP factors in the number of social encounters ($F_{(1, 20)}$ = 5.361, p = 0.031), that was reduced only in the NVHL vehicle-treated group (*post hoc*: p < 0.05; **Fig. 1F**).

Morphological results

Effects of RISP on neuronal morphology and dendritic spine dynamics impairments in the PFC due to NVHL.

The basal dendritic arbor length, dendritic spine density and dendritic spine morphological classification of 640 pyramidal neurons from PFC layers 3 and 5 was carried out (**Fig. 2**). In the PFC layer 3 neurons, the NVHL reduced their total dendritic length ($F_{(1, 28)}$ = 9.431, p = 0.004) and RISP treatment increased it ($F_{(1, 28)}$ = 5.869, p = 0.022; **Fig. 3A**). The decrease in the dendritic arbor was because of the reduction of the 2nd and 3rd order dendrites length only in the NVHL-vehicle group (interaction: $F_{(18, 196)}$ = 2.396, p = 0.002; lesion: $F_{(3, 196)}$ = 7.079, p < 0.001; dendritic order: $F_{(6, 196)}$ = 526.2, p < 0.001) and RISP treatment restored the length of both orders in NVHL animals (*post hoc*: 2nd order, p < 0.01; 3rd order, p < 0.001; **Fig. 3B**). Dendritic spine density decreased because of NVHL ($F_{(1, 28)}$ = 4.667, p = 0.039), increased as RISP effect ($F_{(1, 28)}$ = 7.286, p = 0.011), and there was an interaction between factors ($F_{(1, 28)}$ = 9.911, p = 0.004); the decrease in dendritic spine number as a consequence of NVHL got restored after RISP administration according with *post hoc* analyses (p < 0.01; **Fig. 3C**). Regarding the morphological classification of dendritic spines, the mushroom spine population decreased because of NVHL ($F_{(1, 28)}$ = 20.99, p < 0.001) and increased as a consequence of RISP treatment ($F_{(1, 28)}$ = 10.06, p = 0.004; **Fig. 3D**). Also, RISP increased the thin spine population ($F_{(1, 28)}$ = 26.38, p < 0.001), and the NVHL effect of reducing these kinds of spines was almost significant ($F_{(1, 28)}$ = 4.192, p = 0.052; **Fig. 3D**). In the stubby spine population, not only significant interaction between the lesion and RISP factors was found, but also the number of stubby

JNeurosci Accepted Manuscript

494 spines increased as because of NVHL and decreased because of RISP
495 (interaction: $F_{(1, 28)}$ = 7.049, p = 0.013; lesion: $F_{(1, 28)}$ = 40.03, p < 0.001; RISP: $F_{(1,$
496 $_{28)}$ = 12.20, p = 0.002); *post hoc* analyses revealed that RISP rescued this spine
497 population in the NVHL animals (p < 0.001; **Fig. 3D**). Moreover, RISP decreased
498 the number of bifurcated spines ($F_{(1, 28)}$ = 33.88, p < 0.001), without NVHL effect
499 ($F_{(1, 28)}$ = 1.962, p > 0.05; **Fig. 3D**). The NVHL increased the number of multi-
500 headed spines and RISP reduced them, also an interaction between the lesion and
501 RISP was found (interaction: $F_{(1, 28)}$ = 15.17, p < 0.001; lesion: $F_{(1, 28)}$ = 40.56, p <
502 0.001; RISP: $F_{(1, 28)}$ = 28.94, p < 0.001); *post hoc* analyses identified that RISP
503 recovered the multi-headed spine population in NVHL animals (p < 0.001; **Fig. 3D**).
504 NVHL increased and RISP decreased the number of unclassified spines (lesion:
505 $F_{(1, 28)}$ = 13.69, p < 0.001; RISP: $F_{(1, 28)}$ = 38.02, p < 0.001; **Fig. 3D**).

506 Regarding PFC layer 5, RISP increased the total dendritic length of these neurons
507 ($F_{(1, 28)}$ = 10.35, p = 0.003) without a NVHL effect ($F_{(1, 28)}$ = 3.077, p = 0.09), also an
508 interaction between factors was almost significant ($F_{(1, 28)}$ = 4.05, p = 0.054); in that
509 sense, *post hoc* analyses were made and revealed that RISP rescued the dendritic
510 length in NVHL animals (p < 0.05; **Fig. 4A**). The branch order analysis exposed
511 that NVHL-vehicle rats had reduced the length of the 2nd, 3rd and 4th branch
512 orders (interaction: $F_{(18, 196)}$ = 2.094, p = 0.007; lesion: $F_{(3, 196)}$ = 13.85, p < 0.001;
513 dendritic order: $F_{(6, 196)}$ = 495.0, p < 0.001), and RISP recovered all of them (*post*
514 *hoc*: 2nd order, p < 0.05; 3rd and 4th orders, p < 0.001; **Fig. 4B**). Also in this layer,
515 an interaction between lesion and RISP was found in dendritic spine density ($F_{(1, 28)}$
516 = 13.57, p = 0.001), *post hoc* analyses identified that RISP recovered the spine
517 density in NVHL animals (p < 0.01; **Fig. 4C**). About dendritic spine morphological
518 classification, mushroom spine population decreased in NVHL animals ($F_{(1, 28)}$ =
519 14.2, p < 0.001) and RISP treatment increased thesekinds of spines ($F_{(1, 28)}$ = 5.6,
520 p = 0.025), also interaction between factors was almost significant ($F_{(1, 28)}$ = 4.1, p =
521 0.052; **Fig. 4D**); in such a manner, *post hoc* test was made and revealed that RISP
522 recovered the number of mushroom spines in the NVHL rats (p < 0.01; **Fig. 4D**).
523 The stubby spine population increased because of NVHL and decreased as a
524 RISP effect, but also a significant interaction between lesion and RISP was found

JNeurosci Accepted Manuscript

(interaction: $F_{(1, 28)}$ = 7.154, p = 0.012; lesion: $F_{(1, 28)}$ = 6.912, p = 0.014; RISP: $F_{(1, 28)}$ = 11.75, p = 0.002); the *post hoc* test identified that RISP recovered the population of these spines in NVHL animals (p < 0.001; **Fig. 4D**). There were no NVHL or RISP effects on thin, bifurcated and multi-headed spines population (**Fig. 4D**). NVHL decreased and RISP increased unclassified spine population (lesion: $F_{(1, 28)}$ = 5.025, p = 0.033; RISP: $F_{(1, 28)}$ = 5.725, p = 0.024; **Fig. 4D**).

Effects of RISP on cell density in the PFC due to NVHL.

NVHL reduced the number of cells in the PFC Cg1 area, without RISP effect (lesion: $F_{(1, 12)}$ = 30.43, p < 0.001; RISP: $F_{(1, 12)}$ = 2.745, p > 0.05; **Fig 5B**).

Effects of NVHL and RISP treatment on neuronal plasticity-associated molecular pathways in the PFC.

The brain-derived neurotrophic factor (BDNF) and its interaction with the tropomyosin-receptor-kinase receptor B (TrkB) is implicated in neuronal plasticity. BNDF protein levels remained unchanged among groups (**Fig 6A**). Two isoforms of TrkB were analyzed, the full-length one (TrKB-FL) which increased because of RISP ($F_{(1, 16)}$ = 10.36, p = 0.005) and there was a trend of the NVHL to reduce it ($F_{(1, 16)}$ = 4.020, p = 0.062; **Fig. 6B**); and the truncated isoform glycoprotein-95 (TrkB-T1) whose levels remained unchanged (**Fig. 6C**). Also, it was calculated a ratio among TrkB-FL/T1, which increased because of RISP ($F_{(1, 16)}$ = 8.610, p = 0.01) without NVHL effect ($F_{(1, 16)}$ = 0.4302, p > 0.05; **Fig. 6D**). Within the diverse signaling pathway activated by BDNF/TrkB activity, there are phosphoinositide 3-kinase (PI3K)/protein kinase B (Akt) and mitogen-activated protein kinases (MAPK) pathways. PI3K levels decreased in the rats with NVHL ($F_{(1, 16)}$ = 15.92, p = 0.001), and the RISP increased the levels of this protein ($F_{(1, 16)}$ = 16.26, p = 0.001; **Fig. 6E**). Interaction between lesion and RISP was found in Akt ratio ($F_{(1, 16)}$ = 7.932, p = 0.012), which increased in the NVHL-RISP animals only in comparison with the NVHL-vehicle group (*post hoc*: p < 0.05; **Fig. 6F**). Moreover, a MAPK pathway involved in neuronal plasticity is the one regulated by the extracellular-regulated kinase (ERK). NVHL has no effect on ERK ratio protein levels ($F_{(1, 16)}$ = 0.4513; p >

JNeurosci Accepted Manuscript

0.05), but increased because of RISP ($F_{(1, 16)}$ = 8.889; p = 0.009); also an interaction between lesion and RISP was significant ($F_{(1, 16)}$ = 7.401, p = 0.015) and *post hoc* test analyses showed that RISP recovered the decreased levels of ERK ratio in NVHL animals (p < 0.01; **Fig. 6G**).

Effects of NVHL and RISP treatment on inflammatory and oxidative/nitrosative stress markers in the PFC.

To evaluate the inflammatory state in the PFC, the nuclear factor-kappa B (NF-κB) pathway was studied. The inhibitory subunit of the NF-κB, I kappa B alpha (IκBα), increased because of RISP ($F_{(1, 16)}$ = 8.129, p = 0.012) without NVHL effect ($F_{(1, 16)}$ = 0.1575, p > 0.05; **Fig. 7A**). Neither lesion or RISP treatment affected NF-κB levels (**Fig. 7B**). Also, the cyclooxygenase-2 (COX-2) levels were evaluated, which increased as the main effect of the NVHL ($F_{(1, 16)}$ = 5.278, p = 0.035) and interaction between lesion and RISP was almost significant ($F_{(1, 16)}$ = 4.226, p = 0.056) **Fig. 7C**), in that sense, a *post hoc* test was made and COX-2 levels increased only in NVHL-vehicle group (p < 0.01), thus RISP reduced COX-2 in NVHL animals. Furthermore, the peroxisome proliferator-activated receptor gamma (PPARγ) protein levels were evaluated, which decreased because of the NVHL ($F_{(1, 16)}$ = 11.34, p = 0.004) and RISP did not effect ($F_{(1, 16)}$ = 0.08502, p > 0.05; **Fig. 7D**).

To explore oxidative/nitrosative stress, NO_2^- concentration was examined. NVHL animals had higher NO_2^- levels ($F_{(1, 16)}$ = 5.689, p = 0.029), without RISP effect ($F_{(1, 16)}$ = 3.543, p = 0.078; **Fig. 7E**). Then, neither NVHL or RISP affected the inducible isoform of the nitric oxide synthase (iNOS) levels (**Fig. 7F**). Also, lipid peroxidation markers MDA and 4-hydroxy-2-nonenal (4-HNE) were evaluated. NVHL has no effect on MDA concentration ($F_{(1, 16)}$ = 9.021, p > 0.05) but RISP decreased it ($F_{(1, 16)}$ = 4.592, p = 0.048) and, the interaction between the lesion and RISP was significant ($F_{(1, 16)}$ = 8.106, p = 0.012); the *post hoc* test indicated that RISP reduced the concentration of MDA in NVHL animals (p < 0.05; **Fig. 7G**). Moreover, RISP decreased 4-HNE protein levels ($F_{(1, 16)}$ = 11.61, p = 0.004) without the NVHL effect ($F_{(1, 16)}$ = 2.953, p > 0.105; **Fig. 7H**).

JNeurosci Accepted Manuscript

584 Regarding the nuclear factor (erythroid-derived 2)-like 2 (Nrf2) pathway, which is
585 related to the antioxidant response was evaluated. The glycogen synthase kinase
586 3 beta (GSK-3β) modulates the activity of the Kelch-like ECH-associated protein 1
587 (Keap1), which is the cytosolic inhibitor of Nrf2. NVHL increased GSK-3β ratio ($F_{(1,}$
588 $_{16)}$ = 4.975, p = 0.04) and RISP did not modify this ratio ($F_{(1, 16)}$ = 0.3938, p > 0.05;
589 **Fig. 8A**). The same patter effect was observed in Keap1 protein levels, which
590 increased in NVHL animals ($F_{(1, 16)}$ = 10.79, p = 0.005) without RISP effect ($F_{(1, 16)}$ =
591 1.012, p > 0.05); and because the interaction between factors was close
592 significance threshold ($F_{(1, 16)}$ = 3.999, p = 0.063; **Fig. 8B**), a *post hoc* test was
593 made and revealed that RISP reduced Keap1 levels in NVHL animals (p < 0.01).
594 Finally, NVHL decreased the nuclear protein levels of Nrf2 and RISP increased
595 them (lesion: $F_{(1, 16)}$ = 12.53, p = 0.003; RISP: $F_{(1, 16)}$ = 4.937, p = 0.041; **Fig. 8C**).

596 *Effects of NVHL and RISP treatment on inflammatory and oxidative/nitrosative*
597 *stress markers in serum and PBMCs.*

598 The peripheral inflammatory balance was evaluated in PMBC. About the NF-κB
599 pathway, NVHL did not change IκBα levels ($F_{(1, 16)}$ = 0.00249, p > 0.05) however
600 RISP treatment increase them ($F_{(1, 16)}$ = 9.167, p = 0.008; **Fig. 9A**). However, NF-
601 κB protein levels remained unchanged (**Fig. 9B**). Both NVHL and RISP increased
602 COX-2 protein levels (lesion: $F_{(1, 16)}$ = 4.766, p = 0.044; RISP: $F_{(1, 16)}$ = 9.601, p =
603 0.007; **Fig. 9C**). PPARγ protein levels remained unchanged among groups (**Fig.**
604 **9D**). Also NO_2^- and iNOS was explored. NVHL increased NO_2^- concentration ($F_{(1,}$
605 $_{16)}$ = 4.703, p = 0.045) without RISP effect ($F_{(1, 16)}$ = 0.0878, p > 0.05; **Fig. 9E**). For
606 iNOS levels, there was an interaction between lesion and RISP factors ($F_{(1, 16)}$ =
607 4.835, p = 0.043; **Fig. 9F**), however, no differences among groups were significant.
608 Interaction between lesion and RISP was close to the significance threshold for
609 MDA concentration ($F_{(1, 16)}$ = 4.042, p = 0.061), in that sense, the *post hoc* test
610 revealed that RISP reduced MDA concentration in NVHL animals (p < 0.05; **Fig.**
611 **9G**). 4-HNE showed an interaction between factors ($F_{(1, 16)}$ = 7.805, p = 0.013) and
612 RISP treatment decreased the protein levels only in the NVHL rats (*post hoc*: p <
613 0.05; **Fig. 9H**). Finally, regarding the Nrf2 pathway, NVHL increased GSK-3β ratio

JNeurosci Accepted Manuscript

levels ($F_{(1, 16)}$ = 5.839, p = 0.028) and significant interaction between lesion and RISP was found ($F_{(1, 16)}$ = 5.455, p = 0.033), RISP recovered GSK-3β ratio in the NVHL animals (*post hoc*: $p < 0.05$; **Fig. 10A**). However, Keap1 protein levels did not change (**Fig. 10B**). NVHL was closely to be significant as the main effect promoting the increase of Nrf2 protein levels ($F_{(1, 16)}$ = 3.959, p = 0.064) and RISP did not affect them ($F_{(1, 16)}$ = 2.301, $p > 0.05$; **Fig. 10C**).

DISCUSSION

We found that NVHL rats have dendritic arbor and spine pathology in pyramidal cells of the PFC when studied at adulthood. Also, these animals lose cells due to impaired BDNF/TrkB signaling and oxidative/nitrosative stress in this area. Furthermore, adult animals subjected to NVHL exhibit peripheral oxidative/nitrosative stress. 21 consecutive days of RISP treatment (0.25 mg/kg, ip) ameliorated most of those alterations and also corrected behavioral abnormalities observed in the NVHL rats.

PFC dysfunction is associated with the behavioral alterations exhibited by the NVHL rats (O'Donnell, 2012). The novel environment hyperlocomotion of NVHL animals is related to stress vulnerability observed in schizophrenia, and indicates an increase in the ventral striatum dopaminergic tone (Flores et al., 1996; Flores et al., 2005). Therefore, RISP reduced mesolimbic dopaminergic hyperfunction in rats with NVHL, and as a consequence the number of movements during the motor test. Also, the rise in the ventral striatum dopaminergic tone generates a dysregulation in the corticolimbic system due to NAcc GABAergic hyperactivity in the ventral pallidum. This structure regulates the spontaneous activity of the dorsomedial thalamus, and the aforementioned would dysregulate the PFC function (Flores et al., 2016). Also, NVHL rats had poor social interaction, an innate behavior in the rats (Vanderschuren et al., 1997) that can be related to social isolation, a negative symptom of SZ (Wible et al., 2001). Generally, negative symptoms only improve with long antipsychotic treatments (Remington et al., 2016). In our study, RISP only improved the number of social encounters of NVHL animals, maybe because of the duration of the treatment.

JNeurosci Accepted Manuscript

644 Behavioral enhancement as a result of RISP in NVHL rats might have functional
645 and anatomical substrates at the CNS level. Our results demonstrate that PFC
646 pyramidal neurons of NVHL animals are atrophied and have a dendritic spine
647 pathology and RISP treatment ameliorated those morphological alterations.

648 Neural plasticity is regulated by various molecules, including neurotrophic factors
649 such as BDNF. BDNF acts through Trk receptors, and the most abundant isoform
650 in the neocortex is the TrkB, including the TrkB-FL and TrkB-T1 isoforms
651 (Middlemas et al., 1991; Bramham and Messaoudi, 2005). When BDNF interacts
652 with TrkB-FL, it promotes the arborization of the dendritic arbor and spinogenesis
653 (Cohen-Cory et al., 2010); but when it interacts with TrkB-T1 it has an antagonistic
654 effect on TrkB-FL signaling (Carim-Todd et al., 2009). Neither BDNF, TrkB-FL and
655 TrkB-T1 were affected by NVHL. However, RISP increased the TrkB-FL levels in
656 the NVHL rats. Interestingly, a reduction in BDNF mRNA in the PFC of NVHL
657 animals has been observed (Lipska et al., 2001).

658 Alterations in the counterbalancing effect of TrkB-FL and TrkB-T1, assessed by the
659 ratio of TrkB-FL to TrkB-T1 expression (hereafter FL/T1 ratio), have been used as
660 a variable index for describing BDNF receptor expression and has been related to
661 distinct mental disorders (Fenner, 2012), including SZ (Wong et al., 2013;
662 Martinez-Cengotitabengoa et al., 2016). RISP treatment increased the TrkB FL/T1
663 ratio in both sham and NVHL rats.

664 BDNF/TrkB activity stimulates ERK and PI3K/Akt pathways, which represent a
665 potential therapeutic target of much interest in several mental illnesses, such as SZ
666 (Alonso et al., 2004; Yuan et al., 2010; Enriquez-Barreto and Morales, 2016).
667 Phosphorylated ERK immunoreactivity develops rapidly in dendritic regions in long-
668 term potentiation (LTP) phenomena (Dudek and Fields, 2001; Kelleher et al., 2004;
669 Tang and Yasuda, 2017), a cellular substrate for cognitive functions (Ying et al.,
670 2002). For LTP development, an adequate quantity, composition and spatial
671 disposition of post-synaptic density (PSD) are necessary (Bosch et al., 2014;
672 Nicoll, 2017). The PSD is made of several cytoskeleton-related proteins, adhesion
673 molecules, and receptors, including TrkB (Aoki et al., 2000; Sheng and

JNeurosci Accepted Manuscript

Hoogenraad, 2007). As the PSD is specifically located on the spine surface, its expansion results in a bigger head size. In such a manner, there is a correlation between shape and function in the dendritic spines, the mushroom-shaped spines being considered mature spines (Matsuzaki et al., 2004). Thus, ERK activity is not only associated with dendritic spine synaptic function but also novel spine formation and maturation (Tang and Yasuda, 2017). Here we demonstrate that NVHL attenuates ERK in the PFC as demonstrated before (Bychkov et al., 2011), and this could be related to the lack of spines, as well as the reduction of mature spines in PFC neurons.

Increased PI3K/Akt protein levels were also observed in NVHL animals after RISP treatment. The PI3K/Akt pathway is involved in cell survival (Cardone, 1998; Lee et al., 2008), and it's impaired activity described here can be associated with the neural density reduction observed in the NVHL. Although a specific neural population decrease was not studied, since cresyl violet stain only allows us to distinguish between neurons and glia because of their size, a decrease of parvalbumin GABAergic interneurons in the PFC has been demonstrated in the NVHL (Cabungcal et al., 2014). Another factor that can be implicated in the PFC cell loss is oxidative/nitrosative stress.

PI3K/Akt (effector), as well as GSK-3β (inhibitor), regulates the Nrf2 antioxidant pathway (Sandberg et al., 2014). Nrf2 is a nuclear factor that promotes the synthesis of different enzymes, such as glutathione peroxidase and catalase that protects the cells from oxidative/nitrosative stress, and its dysfunction has been reported in SZ (Genc and Genc, 2009). Interestingly, the gene expression of the afore-mentioned enzymes is reduced in the NVHL (Hui et al., 2019), in congruence with the disruption of the Nrf2 pathway reported here. This impaired antioxidant response could promote oxidative/nitrosative stress. In such a manner, we analyze the nitric oxide (NO) system by quantifying NO_2^- levels as well as the inducible nitric oxide synthase (iNOS) (Guix et al., 2005). Here we found that NVHL animals have increased NO_2^- levels in the PFC, in congruence with previous reports (Negrete-Diaz et al., 2010; Bringas et al., 2012), however the source of this NO_2^-

JNeurosci Accepted Manuscript

rise has not been examined yet. iNOS is overexpressed in glial cells in response to inflammatory stimuli and produces a large amount of NO (Galea et al., 1992). NVHL does not have an effect on iNOS protein levels, suggesting that other molecules are implicated in oxidative/nitrosative stress.

COX-2 is a potent inflammatory mediator that activates microglia, and the levels of this protein increased in the NVHL animals (Garden and Moller, 2006). Excessive microglia population and activity has recently been demonstrated in the PFC of NVHL animals (Hui et al., 2019). Thus, it can be proposed that oxidative/nitrosative stress is modulated by microglia in the NVHL. Interestingly, increased microglia activity also can be related to excessive synapse elimination and postsynaptic spine shape modifications (Weinhard et al., 2018), explaining the reduction of mature spines in the NVHL.

Most of the information about inflammation and oxidative/nitrosative stress in SZ is from plasma or PBMC studies. These findings attempt to explore (indirectly) the inflammatory state of the brain and to find biomarkers for the disease (Miller et al., 2011; Fraguas et al., 2018). We analyzed the peripheral inflammation and oxidative/nitrosative stress in the NVHL model. PBMCs of NVHL animals have increased COX-2 protein levels, a common finding between the brain and periphery. COX-2 inhibits the synthesis of 15-deoxy-delta-12,14-prostaglandin J_2 (15d-PGJ_2) and therefore reduces the anti-inflammatory response via PPARγ. Clinical studies have demonstrated that the reduction in 15d-PGJ_2, a potent anti-inflammatory molecule, and the increase in NF-κB activity are associated with SZ (Garcia-Bueno et al., 2014b). Also, the capacity of RISP has been shown to reduce some pro-inflammatory cytokines after lipopolysaccharide stimulus (Chen et al., 2012; Al-Amin et al., 2013). Interestingly, RISP increased COX-2 levels in sham and lesioned animals. This can be related to the capability of RISP to increase membrane omega-3 fatty acid synthesis in erythrocytes and the PFC, contributing to an antioxidant effect (McNamara et al., 2009; McNamara et al., 2011). Thus, further studies must detail the effects of RISP on PBMCs. However, the antioxidant capacity of RISP was revealed in the NVHL, since it was capable of reducing lipid

JNeurosci Accepted Manuscript

peroxidation in the PFC and in PBMCs.

In that sense, aforementioned neurotrophic and antioxidant effects could be common antipsychotic mechanisms that ultimately improve behavioral abnormalities in the NVHL model (Rueter et al., 2004; Negrete-Diaz et al., 2010; Bringas et al., 2012). A schematic abstract of the results is shown in Fig. 11.

In conclusion, RISP ameliorates neural PFC abnormalities caused by the NVHL not only due to its monoaminergic antagonist activity, but also by restoring plasticity and reducing the oxidative/nitrosative stress. Then, PFC function improves and, as a consequence, the behavior of the animals improve. Moreover, brain inflammatory imbalances and oxidative/nitrosative stress exhibited in the PFC of NVHL animals, and the RISP modulation in these animals, have an association with peripheral markers. This establishes the usefulness of this animal model to explore a linkage between neurodevelopmental and immunological cues relevant for SZ pathophysiology.

AUTHOR CONTRIBUTIONS

HTB, JCL, and GF designed the study and wrote the protocol. HTB, SMP, RAVR, and HCC performed surgeries, drug administration and behavioral tests. HTB, SMP, AJVH, and LG performed neural reconstructions and dendritic spines morphological classification. HTB, RAVR, and MTR performed stereological procedures. HTB, DMH, and KSM performed biochemical experiments. HTB, SMP, RAVR, and GF performed literature searches and analysis. HTB and GF undertook the statistical analysis. HTB and GF wrote the first draft of the manuscript. All contributing authors have approved the final manuscript.

REFERENCES

Al-Amin MM, Nasir Uddin MM, Mahmud Reza H (2013) Effects of antipsychotics on the inflammatory response system of patients with schizophrenia in peripheral blood mononuclear cell cultures. Clinical psychopharmacology

JNeurosci Accepted Manuscript

764 and neuroscience : the official scientific journal of the Korean College of
765 Neuropsychopharmacology 11:144-151.
766 Alonso M, Medina JH, Pozzo-Miller L (2004) ERK1/2 activation is necessary for
767 BDNF to increase dendritic spine density in hippocampal CA1 pyramidal
768 neurons. Learning & memory 11:172-178.
769 Alquicer G, Silva-Gomez AB, Peralta F, Flores G (2004) Neonatal ventral
770 hippocampus lesion alters the dopamine content in the limbic regions in
771 postpubertal rats. International journal of developmental neuroscience : the
772 official journal of the International Society for Developmental Neuroscience
773 22:103-111.
774 Alquicer G, Morales-Medina JC, Quirion R, Flores G (2008) Postweaning social
775 isolation enhances morphological changes in the neonatal ventral
776 hippocampal lesion rat model of psychosis. Journal of chemical
777 neuroanatomy 35:179-187.
778 Andreazza AC, Shao L, Wang JF, Young LT (2010) Mitochondrial complex I
779 activity and oxidative damage to mitochondrial proteins in the prefrontal
780 cortex of patients with bipolar disorder. Arch Gen Psychiatry 67:360-368.
781 Andreazza AC, Wang JF, Salmasi F, Shao L, Young LT (2013) Specific subcellular
782 changes in oxidative stress in prefrontal cortex from patients with bipolar
783 disorder. Journal of neurochemistry 127:552-561.
784 Aoki C, Wu K, Elste A, Len G-w, Lin S-y, McAuliffe G, Black IB (2000) Localization
785 of brain-derived neurotrophic factor and trkb receptors to postsynaptic
786 densities of adult rat cerebral cortex. Journal of neuroscience research
787 59:454-463.
788 Bello-Medina PC, Flores G, Quirarte GL, McGaugh JL, Prado Alcala RA (2016)
789 Mushroom spine dynamics in medium spiny neurons of dorsal striatum
790 associated with memory of moderate and intense training. Proceedings of
791 the National Academy of Sciences of the United States of America
792 113:E6516-E6525.
793 Bosch M, Castro J, Saneyoshi T, Matsuno H, Sur M, Hayashi Y (2014) Structural
794 and molecular remodeling of dendritic spine substructures during long-term
795 potentiation. Neuron 82:444-459.
796 Bradford MM (1976) A rapid and sensitive method for the quantitation of microgram
797 quantities of protein utilizing the principle of protein-dye binding. Analytical
798 Biochemistry 72:248-254.
799 Bramham CR, Messaoudi E (2005) BDNF function in adult synaptic plasticity: the
800 synaptic consolidation hypothesis. Progress in neurobiology 76:99-125.
801 Bringas ME, Morales-Medina JC, Flores-Vivaldo Y, Negrete-Diaz JV, Aguilar-
802 Alonso P, Leon-Chavez BA, Lazcano-Ortiz Z, Monroy E, Rodriguez-Moreno
803 A, Quirion R, Flores G (2012) Clozapine administration reverses behavioral,
804 neuronal, and nitric oxide disturbances in the neonatal ventral hippocampus
805 rat. Neuropharmacology 62:1848-1857.
806 Brinholi FF, Farias CC, Bonifacio KL, Higachi L, Casagrande R, Moreira EG,
807 Barbosa DS (2016) Clozapine and olanzapine are better antioxidants than
808 haloperidol, quetiapine, risperidone and ziprasidone in in vitro models.
809 Biomedicine & pharmacotherapy = Biomedecine & pharmacotherapie
810 81:411-415.

JNeurosci Accepted Manuscript

811 Brusco J, Dall'Oglio A, Rocha LB, Rossi MA, Moreira JE, Rasia-Filho AA (2010)
812 Descriptive findings on the morphology of dendritic spines in the rat medial
813 amygdala. Neuroscience letters 483:152-156.
814 Bychkov E, Ahmed MR, Gurevich EV (2011) Sex differences in the activity of
815 signalling pathways and expression of G-protein-coupled receptor kinases in
816 the neonatal ventral hippocampal lesion model of schizophrenia. The
817 international journal of neuropsychopharmacology 14:1-15.
818 Cabungcal JH, Counotte DS, Lewis E, Tejeda HA, Piantadosi P, Pollock C,
819 Calhoon GG, Sullivan E, Presgraves E, Kil J, Hong LE, Cuenod M, Do KQ,
820 O'Donnell P (2014) Juvenile antioxidant treatment prevents adult deficits in
821 a developmental model of schizophrenia. Neuron 83:1073-1084.
822 Cardone MH (1998) Regulation of Cell Death Protease Caspase-9 by
823 Phosphorylation. Science 282:1318-1321.
824 Carim-Todd L, Bath KG, Fulgenzi G, Yanpallewar S, Jing D, Barrick CA, Becker J,
825 Buckley H, Dorsey SG, Lee FS, Tessarollo L (2009) Endogenous truncated
826 TrkB.T1 receptor regulates neuronal complexity and TrkB kinase receptor
827 function in vivo. The Journal of neuroscience : the official journal of the
828 Society for Neuroscience 29:678-685.
829 Castellano O, Arji M, Sancho C, Carro J, Riolobos AS, Molina V, Gomez-Nieto R,
830 de Anchieta de Castro EHJ, Jr., Herrero-Turrion MJ, Lopez DE (2013)
831 Chronic administration of risperidone in a rat model of schizophrenia: a
832 behavioural, morphological and molecular study. Behavioural brain research
833 242:178-190.
834 Chen SL, Lee SY, Chang YH, Chen SH, Chu CH, Tzeng NS, Lee IH, Chen PS,
835 Yeh TL, Huang SY, Yang YK, Lu RB, Hong JS (2012) Inflammation in
836 patients with schizophrenia: the therapeutic benefits of risperidone plus add-
837 on dextromethorphan. Journal of neuroimmune pharmacology : the official
838 journal of the Society on NeuroImmune Pharmacology 7:656-664.
839 Cohen-Cory S, Kidane AH, Shirkey NJ, Marshak S (2010) Brain-derived
840 neurotrophic factor and the development of structural neuronal connectivity.
841 Developmental neurobiology 70:271-288.
842 Das NP, Ratty AK (1987) Studies on the effects of the narcotic alkaloids, cocaine,
843 morphine, and codeine on nonenzymatic lipid peroxidation in rat brain
844 mitochondria. Biochemical Medicine and Metabolic Biology 37:258-264.
845 Dickerson F, Stallings C, Origoni A, Schroeder J, Katsafanas E, Schweinfurth L,
846 Savage C, Khushalani S, Yolken R (2016) Inflammatory Markers in Recent
847 Onset Psychosis and Chronic Schizophrenia. Schizophrenia bulletin 42:134-
848 141.
849 Dudek SM, Fields RD (2001) Mitogen-Activated Protein Kinase/Extracellular
850 Signal-Regulated Kinase Activation in Somatodendritic Compartments:
851 Roles of Action Potentials, Frequency, and Mode of Calcium Entry. The
852 Journal of Neuroscience 21:RC122-RC122.
853 Enriquez-Barreto L, Morales M (2016) The PI3K signaling pathway as a
854 pharmacological target in Autism related disorders and Schizophrenia.
855 Molecular and cellular therapies 4:2.
856 Fenner BM (2012) Truncated TrkB: beyond a dominant negative receptor. Cytokine
857 & growth factor reviews 23:15-24.

JNeurosci Accepted Manuscript

858 File SE (1980) The use of social interaction as a method for detecting anxiolytic
859 activity of chlordiazepoxide-like drugs. Journal of neuroscience methods
860 2:219-238.
861 Flores G, Morales-Medina JC, Diaz A (2016) Neuronal and brain morphological
862 changes in animal models of schizophrenia. Behavioural brain research
863 301:190-203.
864 Flores G, Barbeau D, Quirion R, Srivastava LK (1996) Decreased binding of
865 dopamine D3 receptors in limbic subregions after neonatal bilateral lesion of
866 rat hippocampus. The Journal of neuroscience : the official journal of the
867 Society for Neuroscience 16:2020-2026.
868 Flores G, Alquicer G, Silva-Gomez AB, Zaldivar G, Stewart J, Quirion R,
869 Srivastava LK (2005) Alterations in dendritic morphology of prefrontal
870 cortical and nucleus accumbens neurons in post-pubertal rats after neonatal
871 excitotoxic lesions of the ventral hippocampus. Neuroscience 133:463-470.
872 Fraguas D, Diaz-Caneja CM, Ayora M, Hernandez-Alvarez F, Rodriguez-Quiroga
873 A, Recio S, Leza JC, Arango C (2018) Oxidative Stress and Inflammation in
874 First-Episode Psychosis: A Systematic Review and Meta-analysis.
875 Schizophrenia bulletin.
876 Galea E, Feinstein DL, Reis DJ (1992) Induction of calcium-independent nitric
877 oxide synthase activity in primary rat glial cultures. Proceedings of the
878 National Academy of Sciences 89:10945-10949.
879 Garcia-Bueno B, Gasso P, MacDowell KS, Callado LF, Mas S, Bernardo M,
880 Lafuente A, Meana JJ, Leza JC (2016) Evidence of activation of the Toll-like
881 receptor-4 proinflammatory pathway in patients with schizophrenia. Journal
882 of psychiatry & neuroscience : JPN 41:E46-55.
883 Garcia-Bueno B, Bioque M, MacDowell KS, Santabarbara J, Martinez-
884 Cengotitabengoa M, Moreno C, Saiz PA, Berrocoso E, Gasso P, Fe
885 Barcones M, Gonzalez-Pinto A, Parellada M, Bobes J, Mico JA, Bernardo
886 M, Leza JC, Flamm-Peps study CdIBeRdSMS (2014a) Pro-
887 /antiinflammatory dysregulation in early psychosis: results from a 1-year
888 follow-up study. The international journal of neuropsychopharmacology 18.
889 Garcia-Bueno B, Bioque M, Mac-Dowell KS, Barcones MF, Martinez-
890 Cengotitabengoa M, Pina-Camacho L, Rodriguez-Jimenez R, Saiz PA,
891 Castro C, Lafuente A, Santabarbara J, Gonzalez-Pinto A, Parellada M,
892 Rubio G, Garcia-Portilla MP, Mico JA, Bernardo M, Leza JC (2014b) Pro-
893 /anti-inflammatory dysregulation in patients with first episode of psychosis:
894 toward an integrative inflammatory hypothesis of schizophrenia.
895 Schizophrenia bulletin 40:376-387.
896 Garden GA, Moller T (2006) Microglia biology in health and disease. Journal of
897 neuroimmune pharmacology : the official journal of the Society on
898 NeuroImmune Pharmacology 1:127-137.
899 Garey LJ, Ong WY, Patel TS, Kanani M, Davis A, Mortimer AM, Barnes TR, Hirsch
900 SR (1998) Reduced dendritic spine density on cerebral cortical pyramidal
901 neurons in schizophrenia. J Neurol Neurosurg Psychiatry 65:446-453.
902 Genc K, Genc S (2009) Oxidative stress and dysregulated Nrf2 activation in the
903 pathogenesis of schizophrenia. Bioscience Hypotheses 2:16-18.

JNeurosci Accepted Manuscript

Gibb R, Kolb B (1998) A method for vibratome sectioning of Golgi-Cox stained whole rat brain. Journal of neuroscience methods 79:1-4.

Glantz LA, Lewis DA (2000) Decreased dendritic spine density on prefrontal cortical pyramidal neurons in schizophrenia. Arch Gen Psychiatry 57:65-73.

Glausier JR, Lewis DA (2013) Dendritic spine pathology in schizophrenia. Neuroscience 251:90-107.

Green LC, Wagner DA, Glogowski J, Skipper PL, Wishnok JS, Tannenbaum SR (1982) Analysis of nitrate, nitrite, and [15N]nitrate in biological fluids. Analytical Biochemistry 126:131-138.

Guix FX, Uribesalgo I, Coma M, Munoz FJ (2005) The physiology and pathophysiology of nitric oxide in the brain. Progress in neurobiology 76:126-152.

Harris KM, Kater SB (1994) Dendritic Spines - Cellular Specializations Imparting Both Stability and Flexibility to Synaptic Function. Annual review of neuroscience 17:341-371.

Hui CW, Bhardwaj SK, Sharma K, Joseph AT, Bisht K, Picard K, Tremblay ME, Srivastava LK (2019) Microglia in the developing prefrontal cortex of rats show dynamic changes following neonatal disconnection of the ventral hippocampus. Neuropharmacology 146:264-275.

Juncal-Ruiz M, Riesco-Davila L, Ortiz-Garcia de la Foz V, Martinez-Garcia O, Ramirez-Bonilla M, Ocejo-Vinals JG, Leza JC, Lopez-Hoyos M, Crespo-Facorro B (2018) Comparison of the anti-inflammatory effect of aripiprazole and risperidone in 75 drug-naive first episode psychosis individuals: A 3months randomized study. Schizophrenia research 202:226-233.

Kelleher RJ, Govindarajan A, Jung H-Y, Kang H, Tonegawa S (2004) Translational Control by MAPK Signaling in Long-Term Synaptic Plasticity and Memory. Cell 116:467-479.

Konopaske GT, Balu DT, Presti KT, Chan G, Benes FM, Coyle JT (2018) Dysbindin-1 contributes to prefrontal cortical dendritic arbor pathology in schizophrenia. Schizophrenia research.

Kuroki T, Nagao N, Nakahara T (2008) Neuropharmacology of second-generation antipsychotic drugs: a validity of the serotonin–dopamine hypothesis. 172:199-212.

Le Pen G, Grottick AJ, Higgins GA, Martin JR, Jenck F, Moreau JL (2000) Spatial and associative learning deficits induced by neonatal excitotoxic hippocampal damage in rats: further evaluation of an animal model of schizophrenia. Behavioural Pharmacology 11:257-268.

Le Pen G, Kew J, Alberati D, Borroni E, Heitz M-P, Moreau J-L (2003) Prepulse inhibition deficits of the startle reflex in neonatal ventral hippocampal–lesioned rats: reversal by glycine and a glycine transporter inhibitor. Biological psychiatry 54:1162-1170.

Lee SB, Xuan Nguyen TL, Choi JW, Lee KH, Cho SW, Liu Z, Ye K, Bae SS, Ahn JY (2008) Nuclear Akt interacts with B23/NPM and protects it from proteolytic cleavage, enhancing cell survival. Proceedings of the National Academy of Sciences of the United States of America 105:16584-16589.

JNeurosci Accepted Manuscript

949 Leza JC, Garcia-Bueno B, Bioque M, Arango C, Parellada M, Do K, O'Donnell P,
950 Bernardo M (2015) Inflammation in schizophrenia: A question of balance.
951 Neuroscience and biobehavioral reviews 55:612-626.
952 Lipska BK, Jaskiw GE, Weinberger DR (1993) Postpubertal emergence of
953 hyperresponsiveness to stress and to amphetamine after neonatal
954 excitotoxic hippocampal damage: a potential animal model of schizophrenia.
955 Neuropsychopharmacology : official publication of the American College of
956 Neuropsychopharmacology 9:67-75.
957 Lipska BK, Khaing ZZ, Weickert CS, Weinberger DR (2001) BDNF mRNA
958 expression in rat hippocampus and prefrontal cortex: effects of neonatal
959 ventral hippocampal damage and antipsychotic drugs. European Journal of
960 Neuroscience 14:135-144.
961 MacDowell KS, Garcia-Bueno B, Madrigal JL, Parellada M, Arango C, Mico JA,
962 Leza JC (2013) Risperidone normalizes increased inflammatory parameters
963 and restores anti-inflammatory pathways in a model of neuroinflammation.
964 The international journal of neuropsychopharmacology 16:121-135.
965 Martin-Hernandez D, Tendilla-Beltran H, Madrigal JLM, Garcia-Bueno B, Leza JC,
966 Caso JR (2019) Chronic Mild Stress Alters Kynurenine Pathways Changing
967 the Glutamate Neurotransmission in Frontal Cortex of Rats. Molecular
968 neurobiology 56:490-501.
969 Martinez-Cengotitabengoa M, MacDowell KS, Alberich S, Diaz FJ, Garcia-Bueno
970 B, Rodriguez-Jimenez R, Bioque M, Berrocoso E, Parellada M, Lobo A, Saiz
971 PA, Matute C, Bernardo M, Gonzalez-Pinto A, Leza JC, PEPs F (2016)
972 BDNF and NGF Signalling in Early Phases of Psychosis: Relationship With
973 Inflammation and Response to Antipsychotics After 1 Year. Schizophrenia
974 bulletin 42:142-151.
975 Matsuzaki M, Honkura N, Ellis-Davies GC, Kasai H (2004) Structural basis of long-
976 term potentiation in single dendritic spines. Nature 429:761-766.
977 McDannald MA, Whitt JP, Calhoon GG, Piantadosi PT, Karlsson RM, O'Donnell P,
978 Schoenbaum G (2011) Impaired reality testing in an animal model of
979 schizophrenia. Biological psychiatry 70:1122-1126.
980 McNamara RK, Jandacek R, Rider T, Tso P (2011) Chronic risperidone normalizes
981 elevated pro-inflammatory cytokine and C-reactive protein production in
982 omega-3 fatty acid deficient rats. European journal of pharmacology
983 652:152-156.
984 McNamara RK, Able JA, Jandacek R, Rider T, Tso P (2009) Chronic risperidone
985 treatment preferentially increases rat erythrocyte and prefrontal cortex
986 omega-3 fatty acid composition: evidence for augmented biosynthesis.
987 Schizophrenia research 107:150-157.
988 Middlemas DS, Lindberg RA, Hunter T (1991) trkB, a neural receptor protein-
989 tyrosine kinase: evidence for a full-length and two truncated receptors.
990 Molecular and Cellular Biology 11:143-153.
991 Miller BJ, Buckley P, Seabolt W, Mellor A, Kirkpatrick B (2011) Meta-analysis of
992 cytokine alterations in schizophrenia: clinical status and antipsychotic
993 effects. Biological psychiatry 70:663-671.
994 Morales-Medina JC, Mejorada A, Romero-Curiel A, Aguilar-Alonso P, Leon-
995 Chavez BA, Gamboa C, Quirion R, Flores G (2008) Neonatal administration

JNeurosci Accepted Manuscript

of N-omega-nitro-L-arginine induces permanent decrease in NO levels and hyperresponsiveness to locomotor activity by D-amphetamine in postpubertal rats. Neuropharmacology 55:1313-1320.

Negrete-Diaz JV, Baltazar-Gaytan E, Bringas ME, Vazquez-Roque RA, Newton S, Aguilar-Alonso P, Leon-Chavez BA, Flores G (2010) Neonatal ventral hippocampus lesion induces increase in nitric oxide [NO] levels which is attenuated by subchronic haloperidol treatment. Synapse 64:941-947.

Nicoll RA (2017) A Brief History of Long-Term Potentiation. Neuron 93:281-290.

Noto C, Ota VK, Gouvea ES, Rizzo LB, Spindola LM, Honda PH, Cordeiro Q, Belangero SI, Bressan RA, Gadelha A, Maes M, Brietzke E (2014) Effects of risperidone on cytokine profile in drug-naive first-episode psychosis. The international journal of neuropsychopharmacology 18.

O'Donnell P (2012) Cortical disinhibition in the neonatal ventral hippocampal lesion model of schizophrenia: new vistas on possible therapeutic approaches. Pharmacology & therapeutics 133:19-25.

Paxinos G, Watson C (1986) The rat brain atlas. In: Academic Press, Inc., San Diego, Calif.

Plum F (1972) Prospects for research on schizophrenia. 3. Neurophysiology. Neurosci Res Program Bull 10:384-388.

Potkin SG, Turner JA, Brown GG, McCarthy G, Greve DN, Glover GH, Manoach DS, Belger A, Diaz M, Wible CG, Ford JM, Mathalon DH, Gollub R, Lauriello J, O'Leary D, van Erp TG, Toga AW, Preda A, Lim KO, Fbirn (2009) Working memory and DLPFC inefficiency in schizophrenia: the FBIRN study. Schizophrenia bulletin 35:19-31.

Remington G, Foussias G, Fervaha G, Agid O, Takeuchi H, Lee J, Hahn M (2016) Treating Negative Symptoms in Schizophrenia: an Update. Current treatment options in psychiatry 3:133-150.

Romero-Pimentel AL, Vazquez-Roque RA, Camacho-Abrego I, Hoffman KL, Linares P, Flores G, Manjarrez E (2014) Histological correlates of N40 auditory evoked potentials in adult rats after neonatal ventral hippocampal lesion: animal model of schizophrenia. Schizophrenia research 159:450-457.

Rueter LE, Ballard ME, Gallagher KB, Basso AM, Curzon P, Kohlhaas KL (2004) Chronic low dose risperidone and clozapine alleviate positive but not negative symptoms in the rat neonatal ventral hippocampal lesion model of schizophrenia. Psychopharmacology 176:312-319.

Ryan RT, Bhardwaj SK, Tse YC, Srivastava LK, Wong TP (2013) Opposing alterations in excitation and inhibition of layer 5 medial prefrontal cortex pyramidal neurons following neonatal ventral hippocampal lesion. Cerebral cortex 23:1198-1207.

Sams-Dodd F, Lipska BK, Weinberger DR (1997) Neonatal lesions of the rat ventral hippocampus result in hyperlocomotion and deficits in social behaviour in adulthood. Psychopharmacology 132:303-310.

Sandberg M, Patil J, D'Angelo B, Weber SG, Mallard C (2014) NRF2-regulation in brain health and disease: implication of cerebral inflammation. Neuropharmacology 79:298-306.

JNeurosci Accepted Manuscript

1042 Sekar A, Bialas AR, de Rivera H, Davis A, Hammond TR, Kamitaki N, Tooley K,
1043 Presumey J, Baum M, Van Doren V, Genovese G, Rose SA, Handsaker
1044 RE, Schizophrenia Working Group of the Psychiatric Genomics C, Daly MJ,
1045 Carroll MC, Stevens B, McCarroll SA (2016) Schizophrenia risk from
1046 complex variation of complement component 4. Nature 530:177-183.
1047 Sellgren CM, Gracias J, Watmuff B, Biag JD, Thanos JM, Whittredge PB, Fu T,
1048 Worringer K, Brown HE, Wang J, Kaykas A, Karmacharya R, Goold CP,
1049 Sheridan SD, Perlis RH (2019) Increased synapse elimination by microglia
1050 in schizophrenia patient-derived models of synaptic pruning. Nature
1051 neuroscience 22:374-385.
1052 Sheng M, Hoogenraad CC (2007) The postsynaptic architecture of excitatory
1053 synapses: a more quantitative view. Annual review of biochemistry 76:823-
1054 847.
1055 Sholl A, Uttley AM (1953) Pattern discrimination and the visual cortex. Nature
1056 171:387-388.
1057 Sierra A, Camacho-Abrego I, Escamilla C, Negrete-Diaz JV, Rodriguez-Sosa L,
1058 Flores G (2009) [Economical body platform for neonatal rats stereotaxic
1059 surgery]. Revista de neurologia 48:141-146.
1060 Tang S, Yasuda R (2017) Imaging ERK and PKA Activation in Single Dendritic
1061 Spines during Structural Plasticity. Neuron 93:1315-1324 e1313.
1062 Tendilla-Beltran H, Antonio Vazquez-Roque R, Judith Vazquez-Hernandez A,
1063 Garces-Ramirez L, Flores G (2019) Exploring the Dendritic Spine Pathology
1064 in a Schizophrenia-related Neurodevelopmental Animal Model.
1065 Neuroscience 396:36-45.
1066 Tseng KY, Chambers RA, Lipska BK (2009) The neonatal ventral hippocampal
1067 lesion as a heuristic neurodevelopmental model of schizophrenia.
1068 Behavioural brain research 204:295-305.
1069 Vanderschuren L, Niesink RJM, Van Pee JM (1997) The neurobiology of social
1070 play behavior in rats. Neuroscience & Biobehavioral Reviews 21:309-326.
1071 Vazquez-Roque RA, Ubhi K, Masliah E, Flores G (2014) Chronic cerebrolysin
1072 administration attenuates neuronal abnormalities in the basolateral
1073 amygdala induced by neonatal ventral hippocampus lesion in the rat.
1074 Synapse 68:31-38.
1075 Vazquez-Roque RA, Ramos B, Tecuatl C, Juarez I, Adame A, de la Cruz F,
1076 Zamudio S, Mena R, Rockenstein E, Masliah E, Flores G (2012) Chronic
1077 administration of the neurotrophic agent cerebrolysin ameliorates the
1078 behavioral and morphological changes induced by neonatal ventral
1079 hippocampus lesion in a rat model of schizophrenia. Journal of
1080 neuroscience research 90:288-306.
1081 Weinberger DR (1987) Implications of Normal Brain Development for the
1082 Pathogenesis of Schizophrenia. Archives of General Psychiatry 44:660.
1083 Weinhard L, di Bartolomei G, Bolasco G, Machado P, Schieber NL, Neniskyte U,
1084 Exiga M, Vadisiute A, Raggioli A, Schertel A, Schwab Y, Gross CT (2018)
1085 Microglia remodel synapses by presynaptic trogocytosis and spine head
1086 filopodia induction. Nature communications 9:1228.
1087 Wible CG, Anderson J, Shenton ME, Kricun A, Hirayasu Y, Tanaka S, Levitt JJ,
1088 O'Donnell BF, Kikinis R, Jolesz FA, McCarley RW (2001) Prefrontal cortex,

JNeurosci Accepted Manuscript

negative symptoms, and schizophrenia: an MRI study. Psychiatry Research: Neuroimaging 108:65-78.

Wong J, Rothmond DA, Webster MJ, Weickert CS (2013) Increases in two truncated TrkB isoforms in the prefrontal cortex of people with schizophrenia. Schizophrenia bulletin 39:130-140.

Ying S-W, Futter M, Rosenblum K, Webber MJ, Hunt SP, Bliss TVP, Bramham CR (2002) Brain-Derived Neurotrophic Factor Induces Long-Term Potentiation in Intact Adult Hippocampus: Requirement for ERK Activation Coupled to CREB and Upregulation ofArcSynthesis. The Journal of Neuroscience 22:1532-1540.

Yuan P, Zhou R, Wang Y, Li X, Li J, Chen G, Guitart X, Manji HK (2010) Altered levels of extracellular signal-regulated kinase signaling proteins in postmortem frontal cortex of individuals with mood disorders and schizophrenia. Journal of affective disorders 124:164-169.

Tables

Parameter	Value
Number of sections (range)	9-15
Distance between sections (μm)	150
Scan grid (μm)	800 X 800
Counting frame (μm)	60 x 60
Disector height (μm)	20
Guard Zones (upper and lower; μm)	10
Average section thickness (μm; range)	35.98 (33.2-38.1)

Table 1. Optical fractionator sampling parameters used for neural counting.

JNeurosci Accepted Manuscript

Figure legends

Figure 1. ***A***, a diagram illustrating the experimental protocol. ***B***, representative coronal photographs of the sham lesion and NVHL, arrows indicate the site of the lesion. ***C***, ***D***, locomotor behavior was evaluated before and after treatment. ***C***, before treatment (n = 24/group), NVHL animals exhibited hyperlocomotion (U = 144, p = 0.002). ***D***, after vehicle or RISP administration (n = 12/group), RISP reduced the number of movements in NVHL rats ($^{\alpha}$lesion effect: $p < 0.001$; $^{\#}p < 0.05$ vs NVHL-RISP, $p < 0.01$ vs sham-RISP, $p < 0.001$ vs sham-vehicle). ***E***, ***F***, social behavior was evaluated only after treatment (n = 6/group). ***E***, NVHL rats spent less time in social behavior and RISP did not affect this parameter ($^{\alpha}$lesion effect: p = 0.001). ***F***, The NVHL reduced the number of social encounters and RISP enhanced the number of encounters (*$p < 0.05$ vs all the other groups). Statistical analyses for locomotor behavior before treatment were conducted using a Mann Whitney U test; for the rest of parameters a two-way ANOVA, Newman Keuls *post hoc* test was used.

Figure 2. ***A***, Representative photomicrographs of the PFC layers 3 and 5 pyramidal neurons from the sham-vehicle group rat (scale bar = 50 μm), ***B***, of dendritic segments of each group (scale bar = 10 μm), and ***C***, examples of each type of dendritic spine according to its shape (scale bar = 2 μm).

Figure 3. NVHL generates neural atrophy in the PFC layer 3 neurons that RISP treatment ameliorated (n = 8/group). ***A***, NVHL reduced the total dendritic length of these neurons and RISP increased it ($^{\alpha}$lesion effect: p = 0.0047; $^{\beta}$RISP effect: p = 0.0221). ***B***, the dendritic arbor length per branch order analysis showed that the NVHL reduced the length of 2nd and 3rd dendritic orders and RISP reversed it ($^{\alpha}$lesion effect: $p < 0.001$; $^{\beta}$RISP effect: $p < 0.001$; $^{\%}p < 0.01$ vs sham-RISP and NVHL-RISP, $p < 0.001$ vs sham-vehicle; $^{\&}p < 0.001$ vs all the other groups). ***C***, concerning dendritic spine density, RISP recovered the number of spines lost by the NVHL ($^{\alpha}$lesion effect: p = 0.039; $^{\beta}$RISP effect: p = 0.012; **$p < 0.01$ vs all the

JNeurosci Accepted Manuscript

other groups). ***D***, NVHL had differential effects on dendritic spine dynamics, since it reduced the number of mushroom and thin spines and increased the stubby, multi-headed and unclassified spines ($^{\alpha}$lesion effect: mushroom, stubby, multi-headed and unclassified $p < 0.001$; thin $p = 0.052$; $^{\#}p < 0.01$ vs sham groups, $p < 0.001$ vs NVHL-RISP). RISP decreased the number of stubby spines and increased the rest of the spine populations ($^{\beta}$RISP effect on stubby spines $p = 0.002$, on mushroom spines $p = 0.004$, on thin, bifurcated, multi-headed and unclassified spines $p < 0.001$). Statistical analyses were conducted using a two-way ANOVA, Newman Keuls *post hoc* test.

Figure 4. NVHL generates neural atrophy in the PFC layer 5 neurons, which RISP treatment ameliorated (n = 8/group). ***A***, RISP increased the total dendritic length of these neurons, and because the interaction between factors was very close to a significant threshold, a *post hoc* test indicated that NVHL animals treated with vehicle had a decreased arbor length that RISP recovered ($^{\beta}$RISP effect: $p = 0.003$; $^{\#}p < 0.05$ vs sham-RISP, $p < 0.01$ vs sham-vehicle and NVHL-RISP). ***B***, the analysis of dendritic arbor length per branch order analysis showed that the NVHL reduced the length of 2nd, 3rd and 4th dendritic orders and RISP reversed it ($^{\alpha}$lesion effect: $p < 0.001$; $^{\beta}$RISP effect: $p = 0.025$; $^{\%}p < 0.05$ vs all the other groups, $^{\&}p < 0.001$ vs all the other groups; $^{\$}p < 0.05$ vs both sham groups and $p < 0.001$ vs NVHL-RISP). ***C***, concerning dendritic spine density, RISP recovered the number of spines lost by the NVHL ($^{+}p < 0.05$ vs sham- RISP, $p < 0.01$ vs sham-vehicle and NVHL-RISP). ***D***, NVHL had differential effects on dendritic spine dynamics, since it reduced the number of mushroom and unclassified spines, and RISP increased both populations (mushroom $^{\alpha}$lesion effect: $p < 0.001$; $^{\beta}$RISP effect: $p < 0.001$; unclassified $^{\alpha}$lesion effect: $p = 0.033$; $^{\beta}$RISP effect: $p = 0.024$). Interaction in the mushroom spine population was very close to the significance threshold and *post hoc* analyses indicated that NVHL vehicle-treated animals had fewer mushroom spines that RISP treatment recovered ($^{@}p < 0.01$ vs NVHL-RISP, $p < 0.001$ vs both sham groups). Stubby spine population increased because of NVHL and decreased as RISP effect ($^{\alpha}$lesion effect: $p = 0.014$; $^{\beta}$RISP effect: $p = 0.002$), a *post*

JNeurosci Accepted Manuscript

hoc test revealed that NVHL vehicle-treated animals had more stubby spines that RISP treatment reduced (***$p < 0.001$ vs all the other groups). Thin, bifurcated and multi-headed spine populations remained unchanged between groups. Statistical analyses were conducted using a two-way ANOVA, Newman Keuls *post hoc* test.

Figure 5. NVHL generate a neural loss in the PFC. ***A***, Representative photomicrographs of cresyl-violet stained brain sections of the region of interest (scale bar = 100 µm). ***B***, NVHL decreased the cell number without a RISP effect (n = 4/group; $^{\alpha}$lesion effect: $p < 0.001$). Statistical analyses were conducted using a two-way ANOVA.

Figure 6. NVHL disrupts the BDNF/TrkB pathway in the PFC. Representative western blot images of each protein and group (n = 5/group). ***A***, BDNF did not change among groups. ***B***, the NVHL effect of reducing TrkB-FL levels was close to significance threshold, however, RISP treatment increased them ($^{\alpha}$lesion effect: $p = 0.062$; $^{\beta}$RISP effect: $p = 0.005$). ***C***, TrkB-T1 remained unchanged among groups. ***D***, TrkB-FL/T1 ratio increased because of RISP ($^{\beta}$RISP effect: $p = 0.001$). ***E***, NVHL reduced PI3K levels and RISP increased them ($^{\alpha}$lesion effect: $p = 0.001$; $^{\beta}$RISP effect: $p = 0.001$). ***F***, Akt increased in the NVHL rats after RISP treatment (*$p < 0.05$ vs NVHL-vehicle). ***G***, RISP increased ERK-ratio levels and recovered the decrease in the NVHL animals ($^{\beta}$RISP effect: $p = 0.009$; $^{\#}p < 0.05$ vs both sham groups, $p < 0.01$ vs NVHL-RISP). Statistical analyses were conducted using a two-way ANOVA, Newman Keuls *post hoc* test.

Figure 7. NVHL generates oxidative/nitrosative stress in the PFC, that RISP treatment ameliorates. Representative western blot images of each protein and group (n = 5/group). ***A***, ***B***, the NF-κB pathway was studied and ***A***, RISP increased IκBα levels ($^{\beta}$RISP effect: $p = 0.012$) but ***B***, neither NVHL or RISP had an effect on NF-κB levels. ***C***, COX-2 increased as a consequence of NVHL and since the interaction between factors was very close to the significance threshold a *post hoc* test was made and revealed that RISP reduced COX-2 levels in the NVHL animals ($^{\alpha}$lesion effect: $p = 0.035$; **$p < 0.01$ vs all the other groups). ***D***, NVHL reduced

JNeurosci Accepted Manuscript

PPAR-γ protein levels ($^{\alpha}$lesion effect: p = 0.004). ***E***, NVHL increased NO_2^- concentration ($^{\alpha}$lesion effect: p = 0.03). ***F***, iNOS levels remained without changes among experimental groups. ***G***, NVHL increased MDA concentration, *post hoc* analyses revealed that MDA concentration decreased because of RISP in NVHL animals ($^{\alpha}$lesion effect: p = 0.012; *p < 0.05 vs all the other groups). ***H***, RISP reduced the 4-HNE levels ($^{\beta}$RISP effect: p = 0.004). Statistical analyses were conducted using a two-way ANOVA, Newman Keuls *post hoc* test.

Figure 8. NVHL impairs the Nrf2 pathway in the PFC of NVHL rats (n = 5/group). ***A***, NVHL increased GSK-3β levels ($^{\alpha}$lesion effect: p = 0.04) ***B***, also NVHL increased Keap1 protein levels, and since the interaction between factors was very close to significance threshold, a *post hoc* test was made and revealed that RISP decreased Keap1 levels in NVHL animals ($^{\alpha}$lesion effect: p = 0.005; $^{\#}p$ < 0.05 vs RISP-treated groups and p < 0.01 vs sham-vehicle). ***C***, NVHL reduced Nrf2 levels and RISP increased them ($^{\alpha}$lesion effect: p = 0.003; $^{\beta}$RISP effect: p = 0.04). Statistical analyses were conducted using a two-way ANOVA, Newman Keuls *post hoc* test.

Figure 9. Oxidative/nitrosative stress was observed in the periphery of NVHL rats (n = 5/group). ***A***, IκBα increased after RISP treatment ($^{\beta}$RISP effect: p = 0.008). ***B***, NF-κB levels remained unchanged. ***C***, COX-2 increased as a consequence of NVHL and RISP treatment ($^{\beta}$RISP effect: p = 0.008). ***D***, PPAR-γ protein levels remained unchanged. ***E***, NO_2^- concentration increased because of NVHL ($^{\alpha}$lesion effect: p = 0.045). ***F***, iNOS protein levels as well as ***G***, MDA concentration remained unchanged among experimental groups. ***H***, RISP reduced the 4-HNE protein levels in NVHL animals (*p < 0.05 vs NVHL-vehicle). Statistical analyses were conducted using a two-way ANOVA, Newman Keuls *post hoc* test.

Figure 10. Evaluation of the Nrf2 pathway in PBMC of NVHL rats (n = 5/group). ***A***, GSK-3β ratio levels increased in NVHL animals and RISP treatment reduced them in these rats ($^{\alpha}$lesion effect: p = 0.028; *p < 0.05 vs all the other groups). ***B***, Keap1 protein levels remained unchanged among groups. ***C***, The RISP effect of

JNeurosci Accepted Manuscript

increasing Nrf2 protein levels was close to the significance threshold ($^{\beta}$RISP effect: $p = 0.064$). Statistical analyses were conducted using a two-way ANOVA, Newman Keuls *post hoc* test.

Figure 11. Schematic abstract of the results. BDNF/TrkB pathway is disrupted in the PFC of NVHL animals as well as the downstream ERK and PI3K/Akt pathways. Also, increased NO_2^-, COX-2 and impaired Nrf2 pathway results in lipid peroxidation (LPO) and oxidative/nitrosative stress. The aforementioned is related to neural atrophy and the dendritic spine pathology in PFC pyramidal cells. RISP had neurotrophic and antioxidant effects restoring BDNF/TrkB and Nrf2 pathways respectively and ultimately ameliorated morphological impairments in the PFC. Oxidative/nitrosative stress can also be detected in the periphery of NVHL rats, and a COX-2 increase was observed both in the PFC and in the PBMC. RISP reduced LPO but increased COX-2 levels in sham animals.

Highlights

- Rats with neonatal ventral hippocampus lesion exhibit behavioral abnormalities that can be associated with schizophrenic symptoms.
- Prefrontal cortex dysfunction underlies behavioral alterations of rats with the neonatal ventral hippocampus lesion.
- Risperidone ameliorates prefrontal cortex neural morphological alterations in the NVHL.
- Risperidone had a neurotrophic effect on the PFC restoring the BDNF/TrkB pathway in the NVHL.
- Oxidative/nitrosative stress in the PFC of NVHL rats is reduced via COX-2 and Nrf2 modulation.
- Peripheral antioxidant effects of RISP was observed in NVHL animals.

JNeurosci Accepted Manuscript

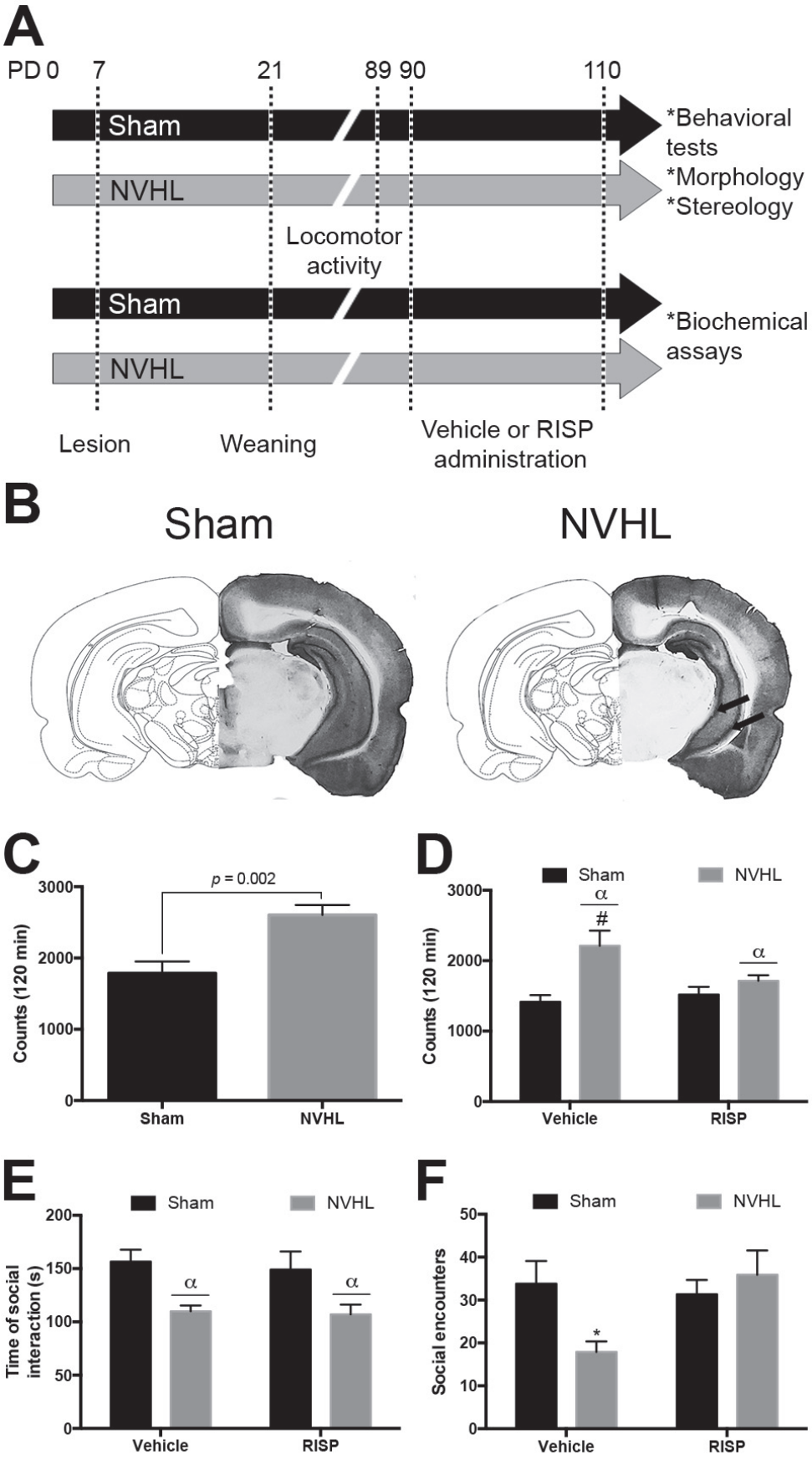

JNeurosci Accepted Manuscript

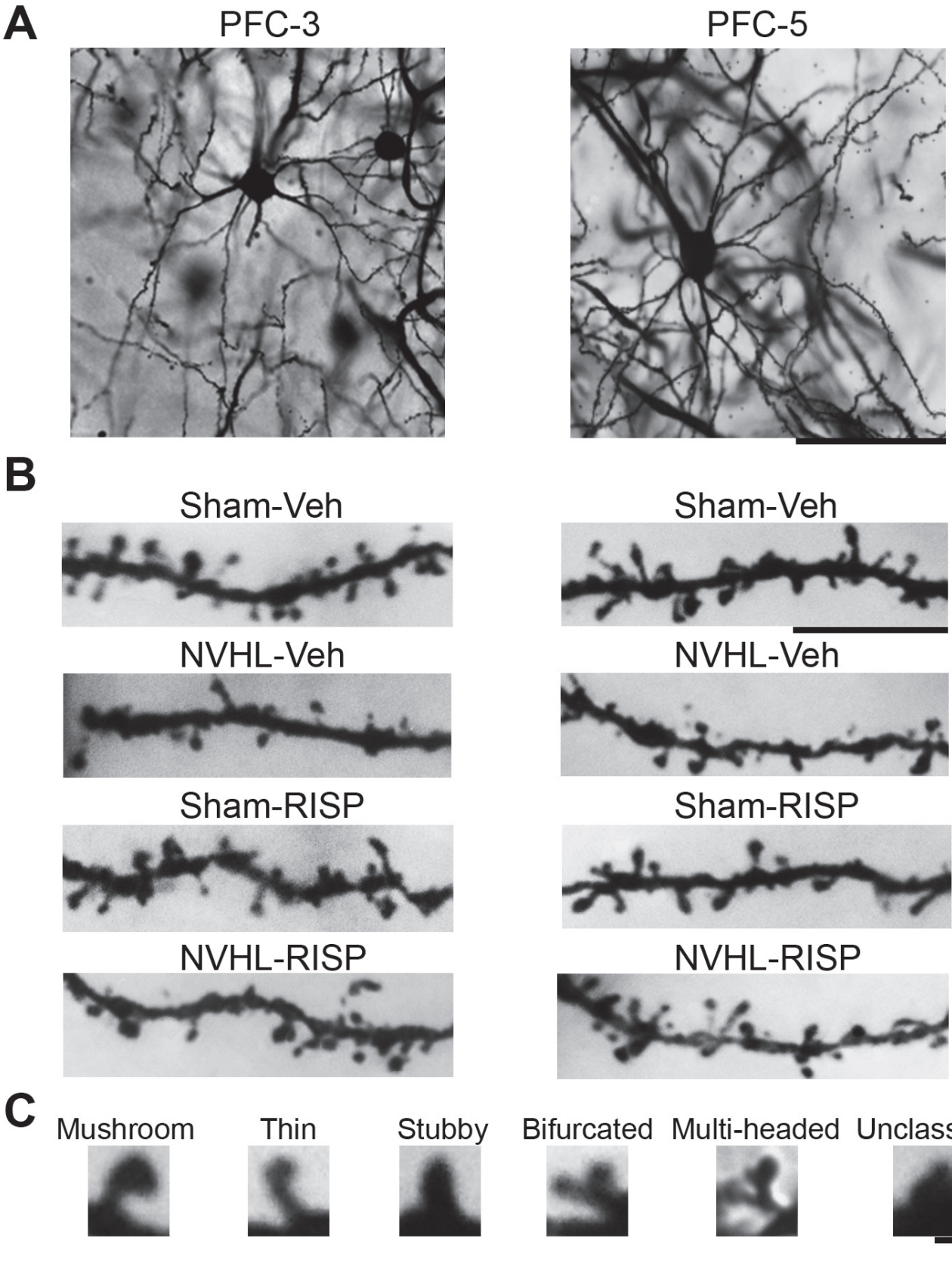

JNeurosci Accepted Manuscript

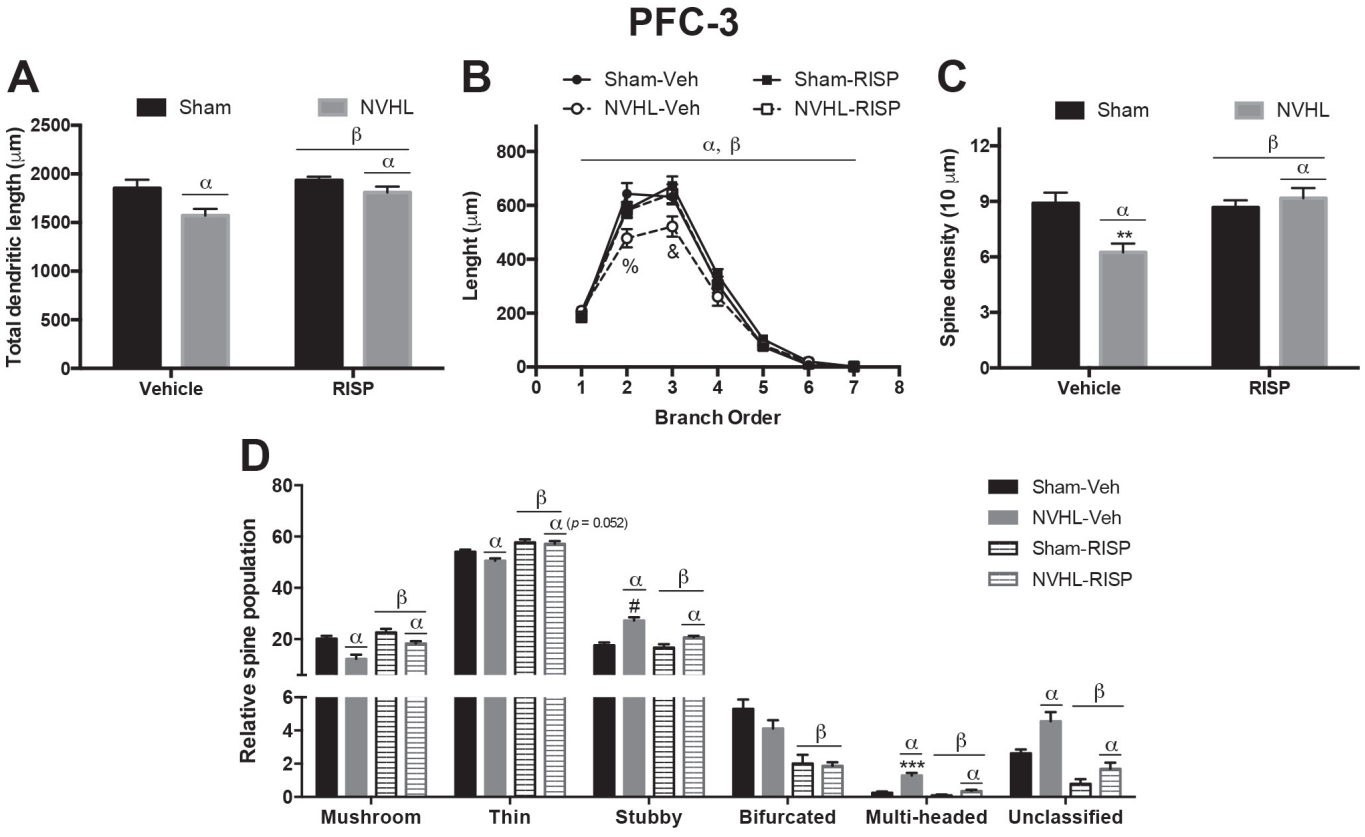

JNeurosci Accepted Manuscript

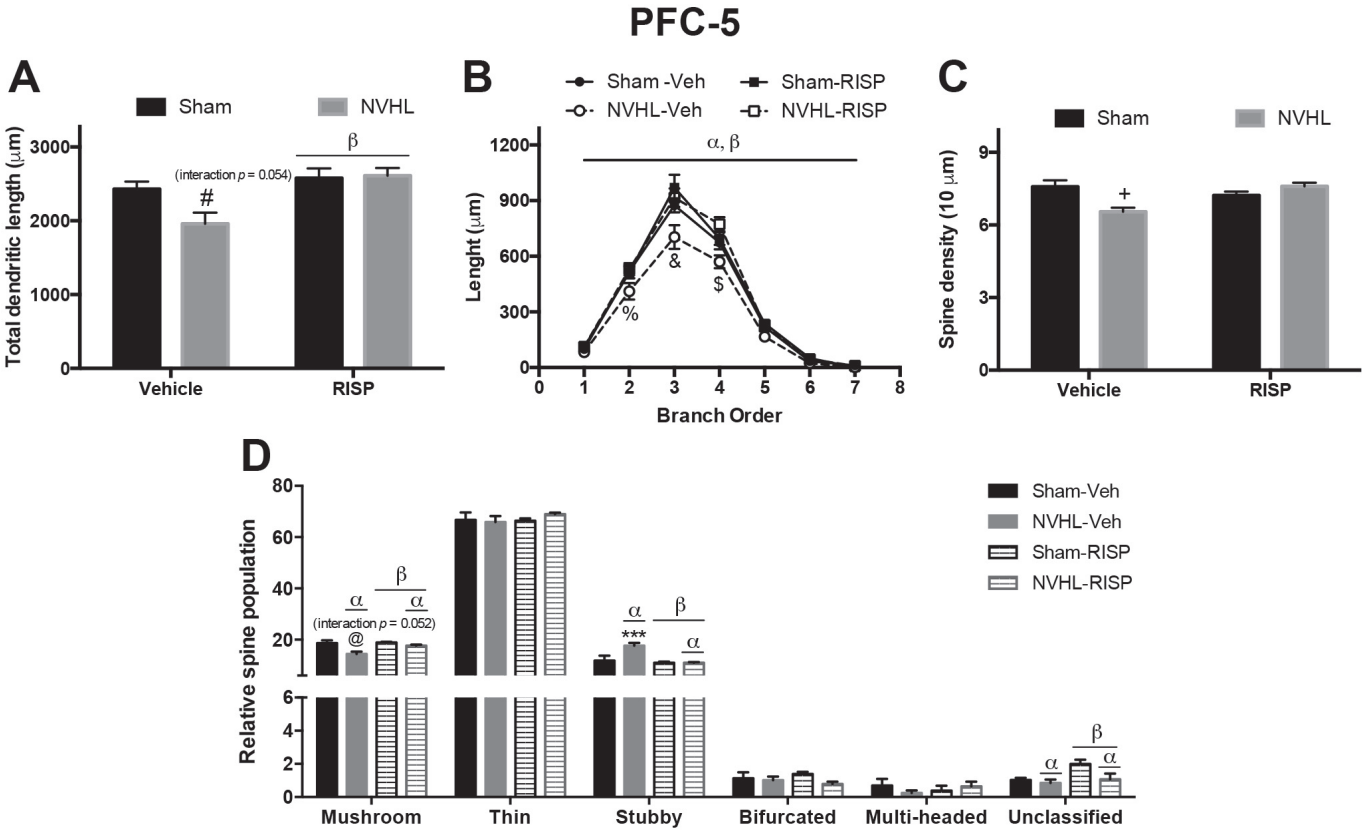

JNeurosci Accepted Manuscript

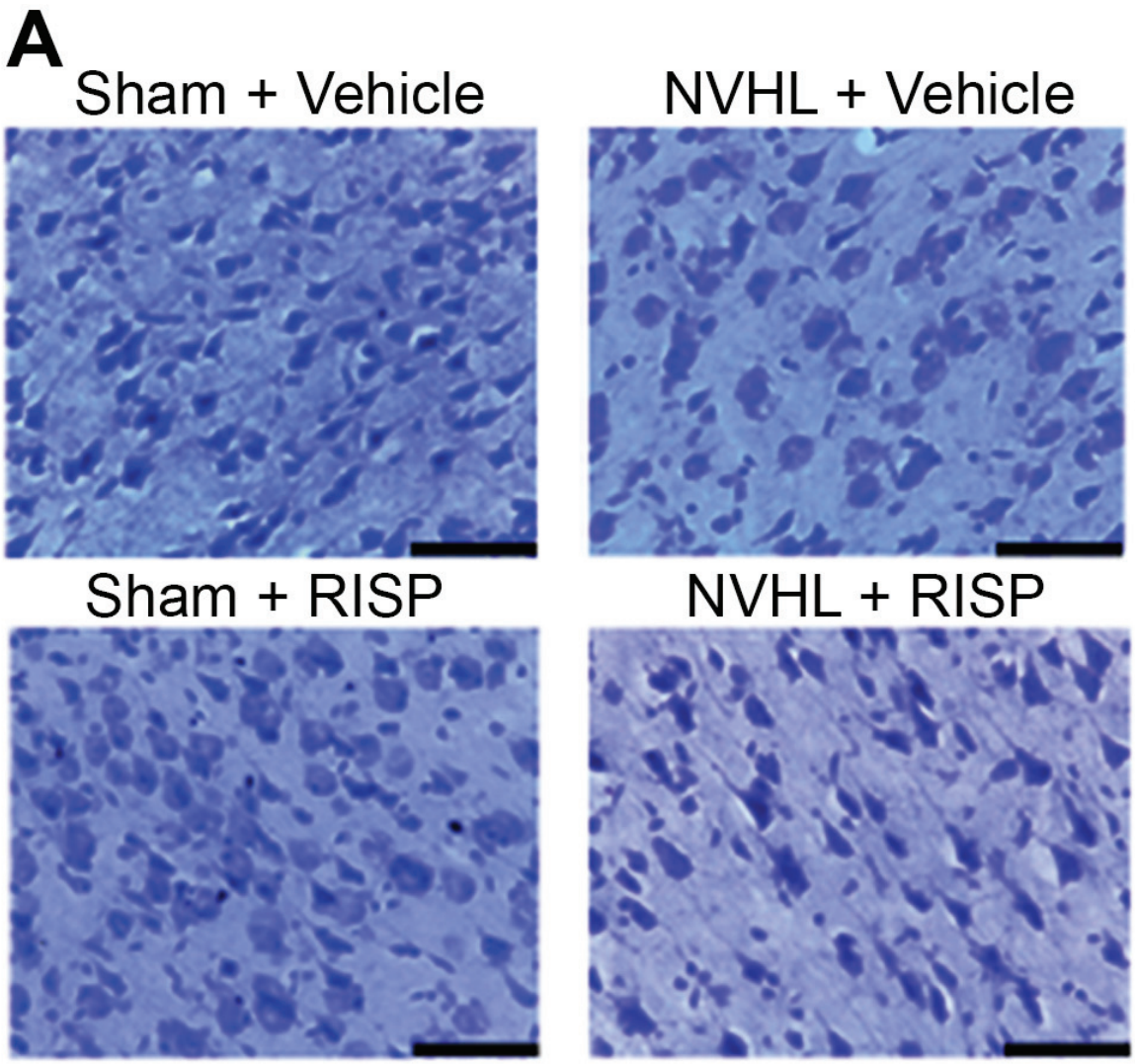

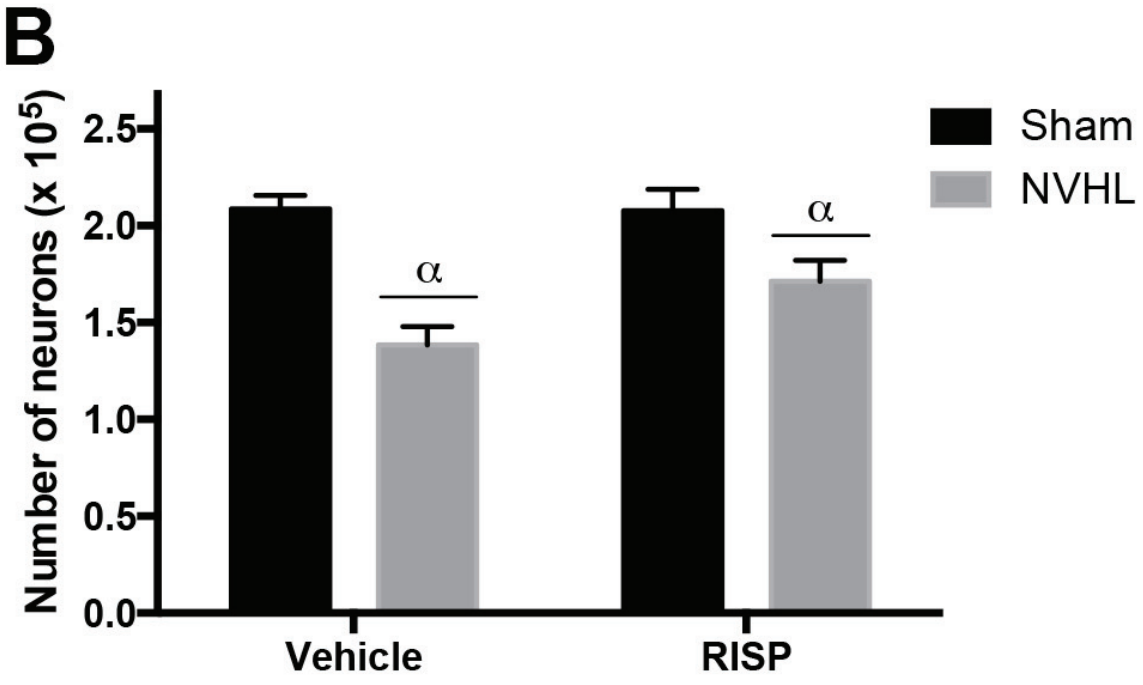

JNeurosci Accepted Manuscript

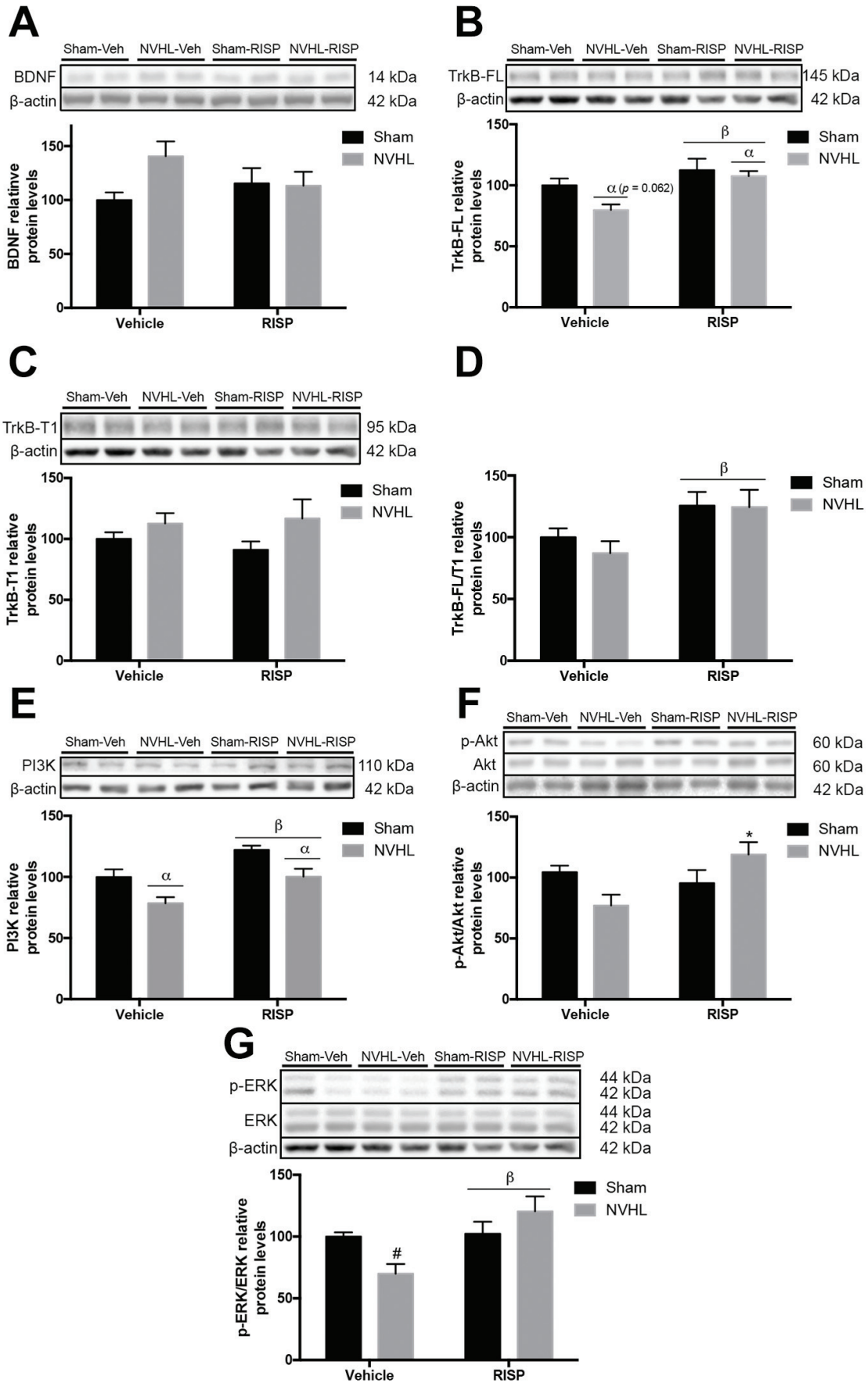

JNeurosci Accepted Manuscript

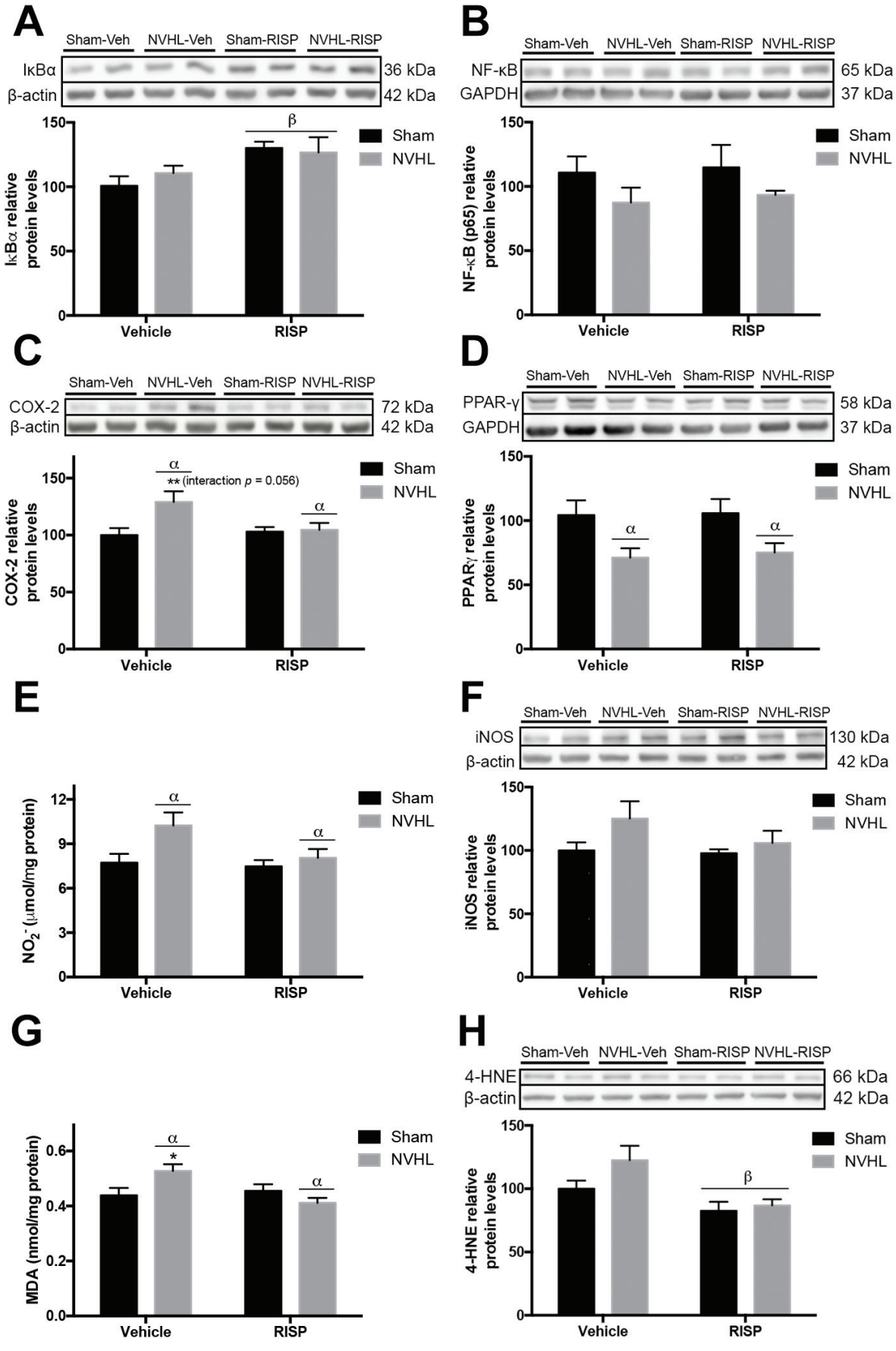

JNeurosci Accepted Manuscript

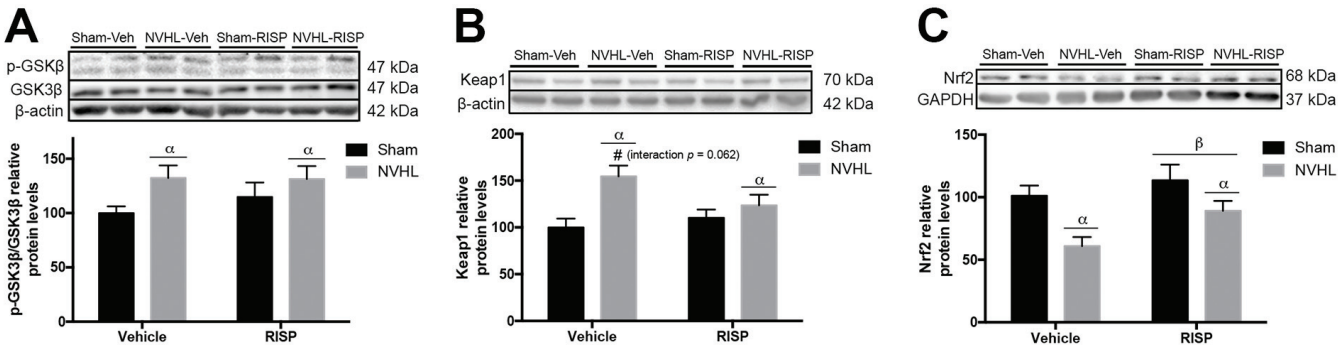

JNeurosci Accepted Manuscript

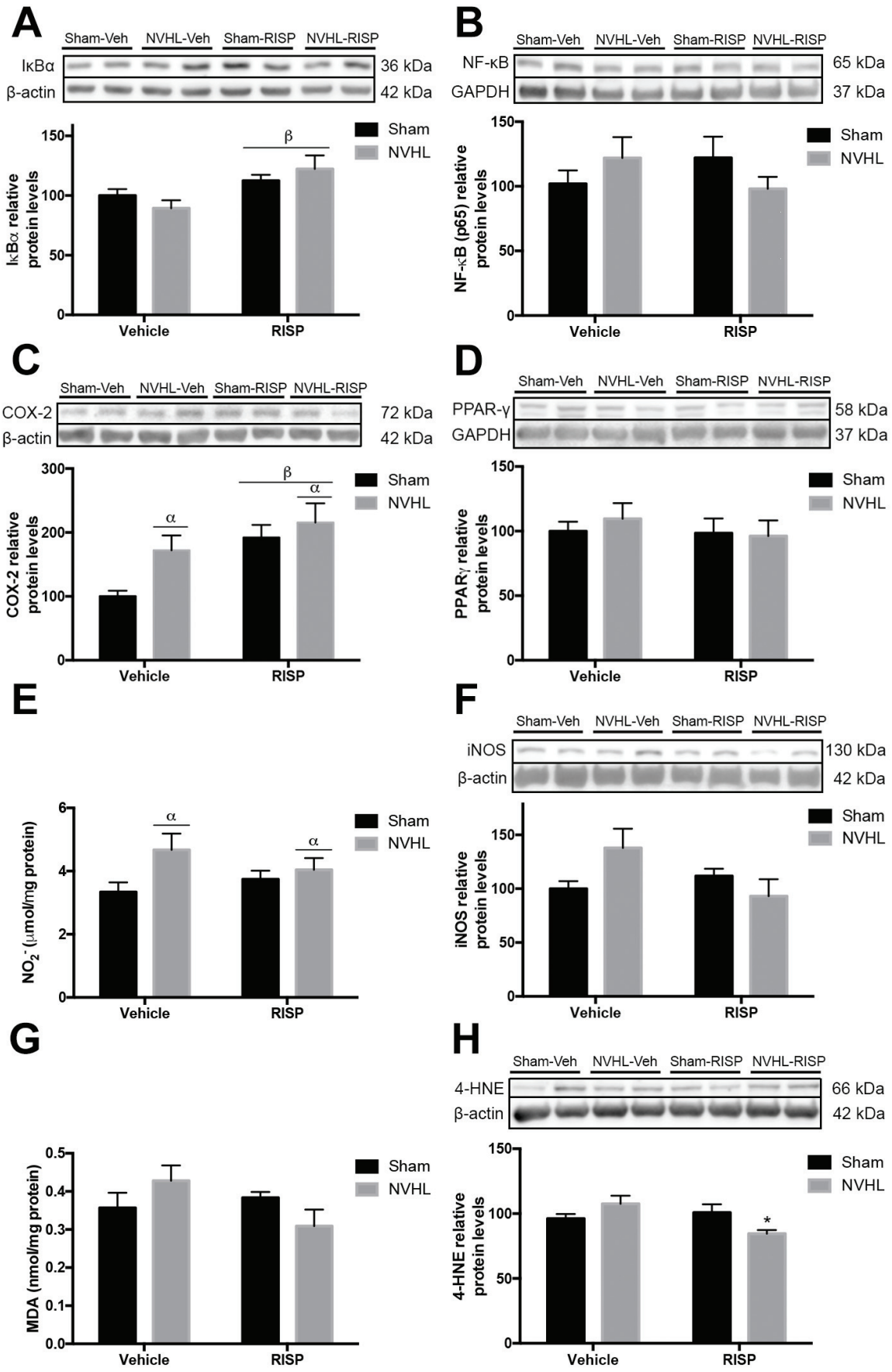

JNeurosci Accepted Manuscript

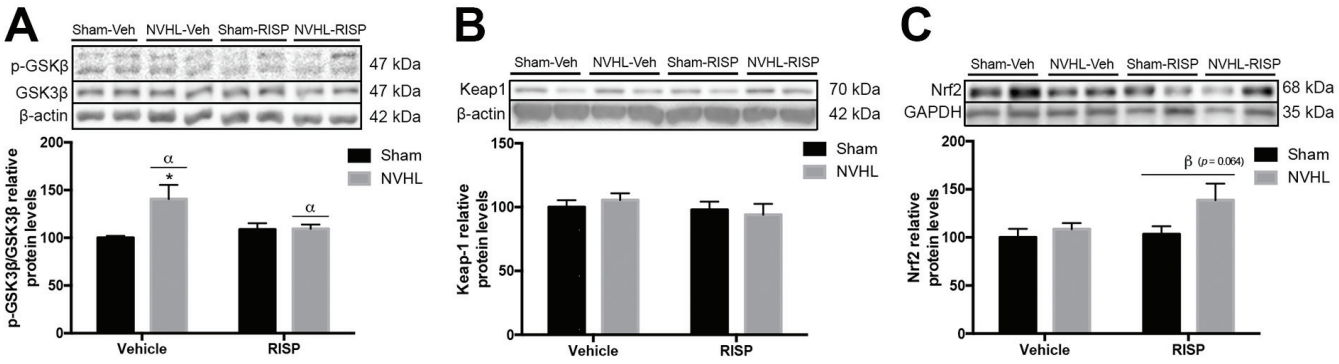

JNeurosci Accepted Manuscript

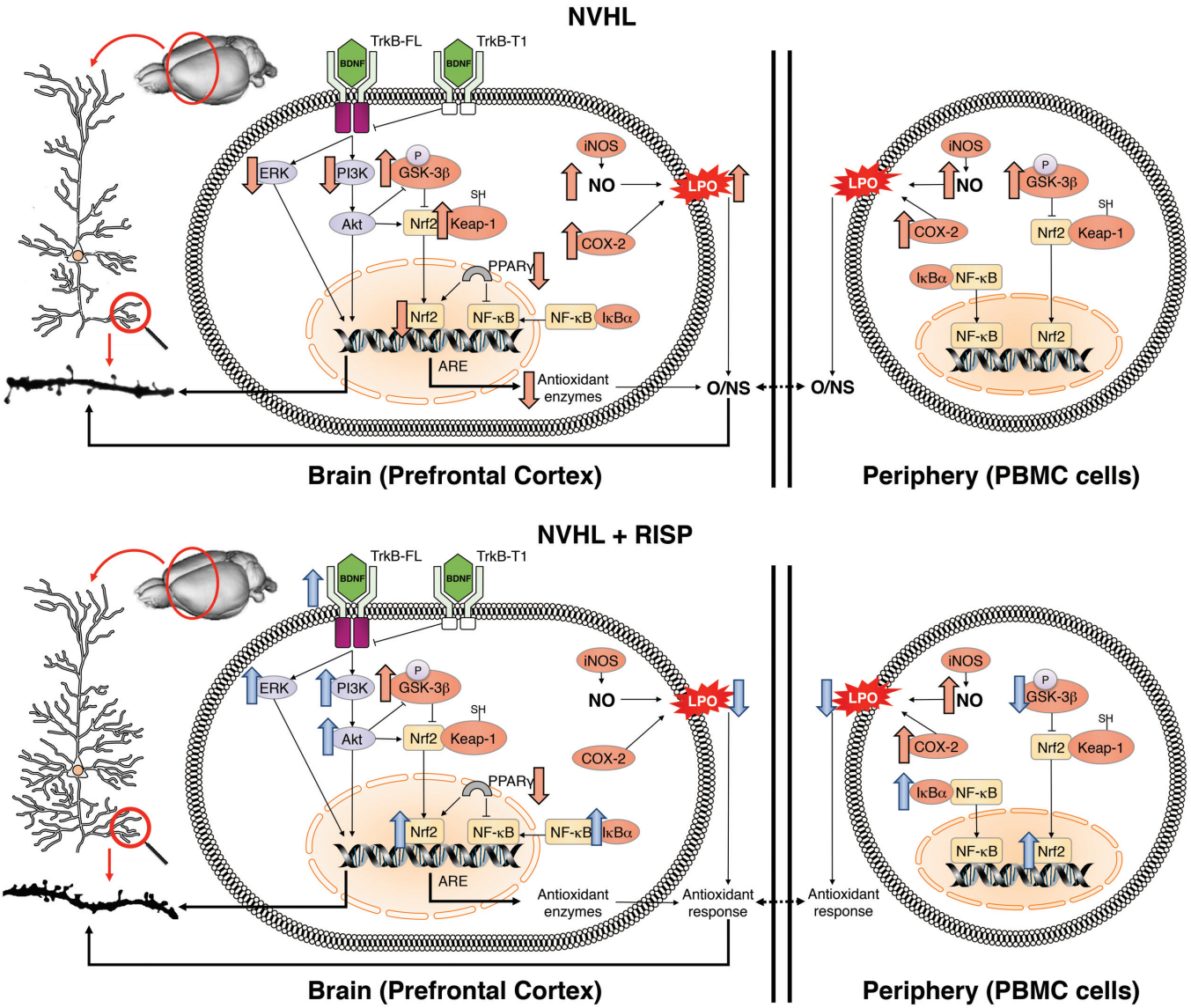

JNeurosci Accepted Manuscript

Table 1. Optical fractionator sampling parameters used for neural counting.

Parameter	Value
Number of sections (range)	9-15
Distance between sections (μm)	150
Scan grid (μm)	800 X 800
Counting frame (μm)	60 x 60
Disector height (μm)	20
Guard Zones (upper and lower; μm)	10
Average section thickness (μm; range)	35.98 (33.2-38.1)